

2016

A Comparison Of FPGA Implementation Of Latency-Based Solvers For Power Electronic System Real-Time Simulation

Matthew Aaron Milton
University of South Carolina

Follow this and additional works at: <http://scholarcommons.sc.edu/etd>

 Part of the [Electrical and Electronics Commons](#)

Recommended Citation

Milton, M. A. (2016). *A Comparison Of FPGA Implementation Of Latency-Based Solvers For Power Electronic System Real-Time Simulation*. (Master's thesis). Retrieved from <http://scholarcommons.sc.edu/etd/3903>

This Open Access Thesis is brought to you for free and open access by Scholar Commons. It has been accepted for inclusion in Theses and Dissertations by an authorized administrator of Scholar Commons. For more information, please contact SCHOLARC@mailbox.sc.edu.

A COMPARISON OF FPGA IMPLEMENTATION OF LATENCY-BASED SOLVERS FOR
POWER ELECTRONIC SYSTEM REAL-TIME SIMULATION

by

Matthew Aaron Milton

Bachelor of Science
University of South Carolina, 2015

Submitted in Partial Fulfillment of the Requirements

For the Degree of Master of Science in

Electrical Engineering

College of Engineering and Computing

University of South Carolina

2016

Accepted by:

Andrea Benigni, Director of Thesis

Jason Bakos, Reader

Cheryl L. Addy, Vice Provost and Dean of The Graduate School

© Copyright by Matthew Aaron Milton, 2016
All Rights Reserved.

ABSTRACT

In the design of power systems, real-time simulation is a powerful tool to evaluate and validate designs before dedicating resources to develop such systems. Through use of real-time simulation, one can study the behavior of a power system in interaction with real, physical elements, all while avoiding the cost and risk in constructing and testing such systems before a design is finalized. In recent decades, effort has been made in the industry and academia to apply real-time simulation to that of switching power converters through use of high-speed digital signal processors (DSPs) and field programmable gate array (FPGA) devices. With these existing approaches, individual converters have been successfully simulated with relatively high switching frequency. At the advent of smart power grids of ever growing size, with switching converters operating at over 100kHz switching frequency, demand has increased to move high-fidelity, real-time simulation from converter-level modeling to system-level to simulate these power systems completely. However, many of the current simulation methods have difficulty to scale to system-level model size while maintaining capability to run in real-time for systems deploying high frequency converters. As such, efforts have been made to explore new simulation approaches that can meet these requirements.

Simulation methods oriented towards high parallelism in their computations are perfect candidates for scalable, system-level real-time simulation. Two such methods include Latency-Based Linear Multi-step Compound Method (LB-LMC) and Latency Insertion Method (LIM). These methods exploit sources of latency in modeled systems to divide up computations into operations that can be performed

simultaneously. Originally developed for software-based execution on traditional processors and DSPs, these methods are implementable on FPGA devices to take advantage of these devices hardware-based, low-latency execution and native parallelism.

In this work, FPGA implementations of the LIM and LB-LMC methods for system-level real-time simulation of power systems are developed and compared for scalability and implementation challenges. FPGA-based simulation engines are developed for both methods on a Xilinx Virtex-7 FPGA evaluation platform. The LB-LMC simulation engine was realized to operate in single or multiple pass execution per simulation time step and apply mixed integration methods for model computations of various electrical components and converters. This engine applies use of subsystem decomposition allowable by LB-LMC to reduce computation time costs and FPGA resources needed for larger power system models. The LIM simulation engine was implemented to operate in a two pass, leapfrog approach to compute simulation solutions every time step. A novel method to handle converter switching action in LIM was developed to enable LIM to model power switching converters. For both simulation engines, various power systems were simulated in real-time with 50ns and below time steps, from a single three-phase converter to an eight converter dual-bus shipboard power system. Simulation accuracy of both methods' FPGA implementation are compared to high precision software-based simulators. The scalability of each method in real-time was analyzed and evaluated in terms of achievable time step, determined by computational delay, and resource usage on an FPGA. Finally, the FPGA implementation of each method is compared for implementation challenges in modeling power systems with these implementations.

TABLE OF CONTENTS

| | |
|---|------|
| ABSTRACT | iii |
| LIST OF TABLES | viii |
| LIST OF FIGURES | ix |
| CHAPTER 1 INTRODUCTION | 1 |
| CHAPTER 2 BACKGROUND | 4 |
| 2.1 Latency-Based Linear Multi-step Compound Method | 4 |
| 2.2 Latency Insertion Method | 7 |
| 2.3 FPGAs and Simulation Computation Implementation | 9 |
| CHAPTER 3 LB-LMC REALIZATION ON FPGA | 13 |
| 3.1 FPGA Encapsulation | 13 |
| 3.2 System Solver Realization | 15 |
| 3.3 Simulation Engine Composition | 18 |
| 3.4 FPGA Implementation | 21 |
| 3.5 Test Models | 22 |
| 3.6 Implementation Results | 24 |

| | | |
|------------|--|----|
| CHAPTER 4 | LIM REALIZATION ON FPGA | 30 |
| 4.1 | FPGA Encapsulation | 30 |
| 4.2 | Simulation Engine Composition | 31 |
| 4.3 | Switching Power Converters in LIM | 32 |
| 4.4 | FPGA Implementation | 38 |
| 4.5 | Implementation Results | 38 |
| CHAPTER 5 | SCALABILITY ANALYSIS | 42 |
| 5.1 | LB-LMC | 43 |
| 5.2 | LIM | 45 |
| 5.3 | Evaluation | 47 |
| CHAPTER 6 | MODELING AND IMPLEMENTATION DISCUSSION | 52 |
| 6.1 | LB-LMC Modeling on FPGA | 52 |
| 6.2 | LIM Modeling on FPGA | 54 |
| CHAPTER 7 | FUTURE WORK | 56 |
| CHAPTER 8 | CONCLUSION | 59 |
| REFERENCES | | 61 |
| APPENDIX A | LB-LMC ENGINE HLS C++ CODE | 63 |
| A.1 | Capacitor Entity | 63 |
| A.2 | Inductor Entity | 64 |
| A.3 | Three Phase Half-Bridge Converter Entity | 64 |

| | |
|---|----|
| A.4 Simulation Engine for Microgrid (Single Bus System) | 66 |
| A.5 System Solver for Microgrid (Single Bus System) | 68 |
| APPENDIX B LIM ENGINE HLS C++ CODE | 73 |
| B.1 Branch Entity | 73 |
| B.2 Node Entity | 73 |
| B.3 Simulation Engine for Microgrid (Single Bus System) | 74 |

LIST OF TABLES

| | | |
|-----------|--|----|
| Table 3.1 | DC/AC Converter Model Parameters | 22 |
| Table 3.2 | Model Error for LB-LMC | 26 |
| Table 3.3 | Resource Usage for Multi-cycle System Solver | 29 |
| Table 4.1 | Model Error for LIM | 39 |
| Table 5.1 | LIM Scalability Results | 49 |
| Table 5.2 | LB-LMC Scalability Results | 50 |

LIST OF FIGURES

| | | |
|-------------|--|----|
| Figure 2.1 | Linear Networks with Nonlinear Components | 4 |
| Figure 2.2 | LB-LMC Solution Flow | 6 |
| Figure 2.3 | LIM Models | 7 |
| Figure 2.4 | LIM Time Base | 8 |
| Figure 2.5 | Diagram of Example FPGA | 9 |
| Figure 2.6 | Hardware Implementation of Difference Equation for LIM Branch Current | 11 |
| Figure 3.1 | Example of DC/AC Converter Component Entity | 14 |
| Figure 3.2 | Separation of Subsystems | 16 |
| Figure 3.3 | LB-LMC Simulation Engine | 19 |
| Figure 3.4 | Finite State Machine for Multi-Cycle Simulation Engine | 20 |
| Figure 3.5 | Three Phase DC/AC Converter | 23 |
| Figure 3.6 | Single Bus Shipboard Power System | 24 |
| Figure 3.7 | Dual Bus Shipboard Power System | 24 |
| Figure 3.8 | Top Level Design for Simulation Platform | 25 |
| Figure 3.9 | Single-Bus Power System Analog Output under LB-LMC | 27 |
| Figure 3.10 | Dual-Bus Power System Analog Output under LB-LMC | 28 |
| Figure 4.1 | FPGA RTL Entities for LIM Models | 31 |

| | | |
|-------------|--|----|
| Figure 4.2 | LIM Simulation Engine FPGA Design | 32 |
| Figure 4.3 | Buck Converter | 33 |
| Figure 4.4 | Buck Converter LIM Model | 33 |
| Figure 4.5 | Buck Converter Switching Action with LIM Model | 34 |
| Figure 4.6 | Three-Phase AC/DC Converter as Inverter | 35 |
| Figure 4.7 | Three-Phase Inverter LIM Model | 35 |
| Figure 4.8 | Handling Switching Action in LIM Simulation Engine | 37 |
| Figure 4.9 | Analog Output for Single-Bus Power System under LIM Engine | 40 |
| Figure 4.10 | Analog Output for Dual-Bus Power System under LIM Engine | 40 |
| Figure 4.11 | Deadband Interval Distortion Result | 41 |
| Figure 5.1 | Scalability Test Model | 48 |
| Figure 5.2 | Plot of LIM Scalability Results | 49 |
| Figure 5.3 | Plot of LB-LMC Scalability Results | 51 |

CHAPTER 1

INTRODUCTION

In the design of power electronic systems, real-time simulation with hardware-in-the-loop (HIL) techniques has in recent decades become an essential tool to evaluation and prototyping of new systems. The development and testing of power electronic systems can be quite risky in terms of cost and safety, especially for high power systems. Real-time simulation with HIL allows developers to reduce these risks by emulating a portion of a system in actual time with a computational device or simulator, and then integrate this emulation with physical elements of the system. Instead of having to construct a prototype of an unproven system portion, one can use the simulation to observe the interaction of a system design with physical components without dealing with the risks and costs of said prototype. Examples of using HIL and real-time simulation for power electronic system applications are found in [1][2][3].

With the use of SiC-based, high-frequency switching converters in modern power electronic systems, operating with switching frequencies of 100-200kHz and greater, the need for small real-time simulation time steps to capture their nonlinear dynamics has become a concern. These small time steps put tight time constraints of the computational device used for the simulation. As such, a change has occurred to move simulation from traditional computer processors to Digital Signal Processors (DSPs) and Field Programmable Gate Arrays (FPGAs) which can compute for smaller time steps in real-time. In recent literature, various power elements have been simulated entirely on FPGA, including a general power con-

verter, induction machine, and transformer [4][5][6], while a MMC converter has been simulated with a CPU-and-FPGA mixed platform [7].

As the expansion of smart grids has grown in recent times, interest has increased for real-time simulation for whole power electronic systems and grid-connected power converters. Examples of current simulation work in this regard are found in [8][9][10]. Many of these present approaches are not tailored for scalable grid or system-level simulation of large power systems with numerous converters and elements; especially for small time steps in real-time. Due to this situation, effort has been made to develop methods for system-level real-time simulation.

For system-level, real-time simulation of modern power electronic systems, scalable solver methods are needed to perform simulation of large models while maintaining small time steps for high frequency dynamics. This scalability can be achieved through the use of methods that exploit parallelism in their operations. One parallelizable simulation method that exists is Latency-Based Linear Multi-step Compound method (LB-LMC), defined in [11]. The LB-LMC method, based on Resistive Companion method, exploits latency in components to separate them from the system solution. This separation allows the components to be solved in parallel before the system solver is complete. Besides the parallelism, LB-LMC is suitable for real-time simulation due to predictable time steps, enabled by pushing nonlinear elements into the components (which typically requires iterative solving) and keeps the system solving side linear. Another method that fits parallel execution well for real-time simulation is Latency Insertion Method (LIM), first described in [12]. In LIM, circuits are modeled as branches and nodes with latency inserted into each one. Applying this latency, the solutions for branches and nodes can be separated and solved in parallel. All branches of a modeled system are solved in parallel in one half time step and then the nodes are solved

all simultaneously in the remaining half time step. Solving the components with non-iterative, explicit integration methods, the time step of LIM execution is foreseeable, making the method suitable for real-time execution like as with LB-LMC method. To maximize parallelism and minimize computational delays for real-time simulation, these methods can be readily implemented on FPGA devices to exploit their native parallel execution and low hardware latencies, enabling time steps below 50ns.

In this work, FPGA implementations of the LIM and LB-LMC methods for system-level real-time simulation of power systems are developed and compared for scalability and implementation challenges. Within Chapter 2, a brief overview of these two simulation methods are discussed, followed by a discussion of FPGAs and implementation of computations for these devices. Then, the FPGA realization of LB-LMC method is presented in Chapter 3, detailing the encapsulation and execution of this method on FPGAs, and providing demonstrating results for this implementation. Afterward, in Chapter 4, the same coverage is given to the FPGA implementation of LIM. With discussion of LB-LMC and LIM FPGA realization covered, the scalability of the two methods in terms of computational delay and resource usage are analyzed and tested, shown in Chapter 5. Finally, a short discussion on challenges and limitations of modeling power electronic systems with these FPGA-implemented simulation methods is given in Chapter 6.

CHAPTER 2

BACKGROUND

2.1 LATENCY-BASED LINEAR MULTI-STEP COMPOUND METHOD

The Latency Based Linear Multi-step Compound Method (LB-LMC) is a highly parallelizable simulation method designed for real-time simulation of dynamic electrical systems. In this section we provide a summary description of this method which is detailed in [11].

The LB-LMC method is derived from the Resistive Companion (RC) method, solving dynamic systems as a set of linear equations $Gx = b$ every simulation time step, where G is the conductances of the system, b is the current contributions of components, and x is the node voltages of the system. Unlike traditional RC method, the LB-LMC method models all nonlinear components in a linear network system as seen in Figure 2.1(a) as functional voltage sources with series resistance

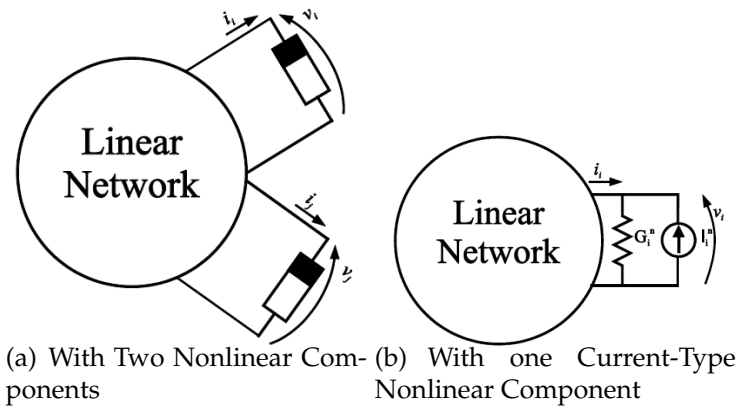


Figure 2.1 Linear Networks with Nonlinear Components

or as shown in Figure 2.1(b), current sources with parallel conductance. These series resistances or parallel conductances are held fixed and are inserted into the G conductance matrix to stay with standard form of RC components. The nonlinear behavior of the nonlinear components are then reflected in the voltage or current source that is updated every simulation step through an internal step that computes the state equation of the component to update said source. The nonlinear component state equations are expressed as:

$$\frac{di_i^n}{dt} = f(v, i, x_i^n, u_i^n, t) \quad (2.1)$$

$$\frac{dv_j^n}{dt} = f(v, i, x_j^n, u_j^n, t) \quad (2.2)$$

, where v is the vector of the network node voltages, i is the vector of the network branch currents, x_i^n is the vector of the state variable internal to the i -th nonlinear component, and u_i is the vector of the input internal to the i -th nonlinear component. Components with multiple terminals can be described by a mix of these current and voltage sources. These equations are explicitly discretized to obtain:

$$I_i^n(k+1) = f(v(k), i(k), x_i^n(k), u_i^n(k), k) \quad (2.3)$$

$$V_j^n(k+1) = f(v(k), i(k), x_j^n(k), u_j^n(k), k) \quad (2.4)$$

Since the state equations for I_i^n and V_j^n are explicitly discretized and only depend on the solutions from previous time step, and the equations are independent from one another, each nonlinear component can perform its internal step in parallel to other components. From these state equations, the source contribution vector b can be updated and the system solution each time step can be found with:

$$Gx(k+1) = b(v(k), i(k), I^n(k), V^n(k), k) \quad (2.5)$$

From having the conductance matrix G held constant due to consisting of only fixed conductances, LU factorization for the LB-LMC method system solver can

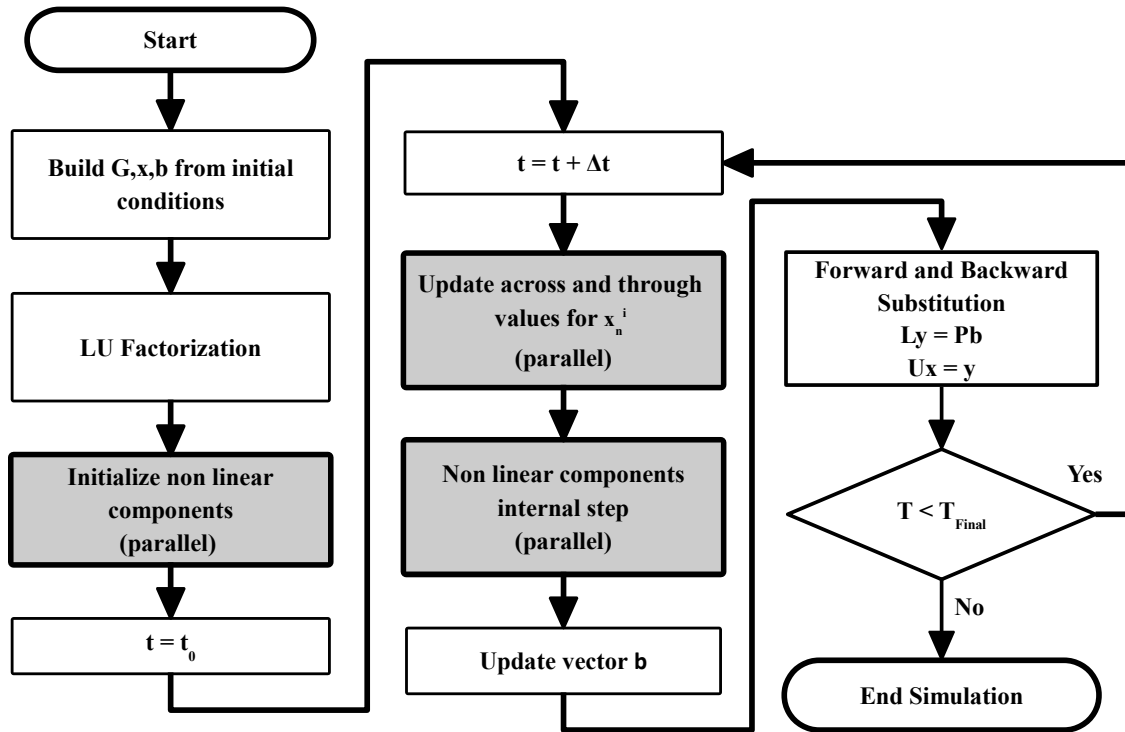


Figure 2.2 LB-LMC Solution Flow

be performed offline, and only forward and backward substitution to solve the system is performed each time step.

Figure 2.2 shows the solution flow for LB-LMC. In this flow, G , x , and b are built from initial conditions and the LU factorization of the conductance matrix is performed. Once all non-linear components are initialized, the simulation loop begins. Each iteration consists of each component performing its own internal step in parallel, then the source vector b is updated. From the updated b vector, the system solution x is computed via forward and backward substitution and saved for the next step. The simulation loop continues until final simulation time is reached.

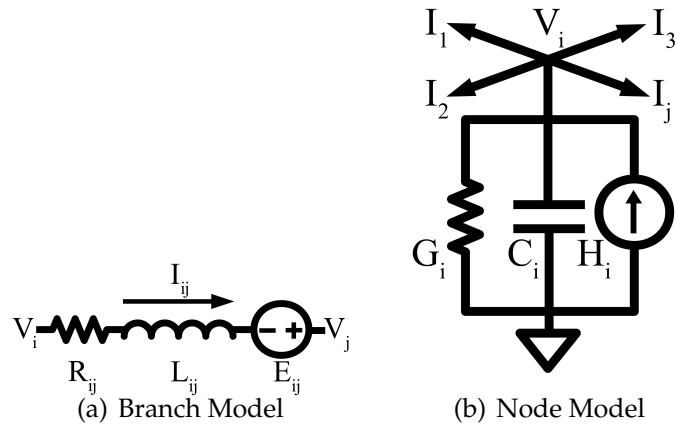


Figure 2.3 LIM Models

2.2 LATENCY INSERTION METHOD

LIM is a finite difference method for transient circuit simulation, first defined in [12]. Beginning with a circuit having no latency, say a resistive network, reactive latency is then inserted into all branches and nodes of a circuit so that branch currents and node voltages both become continuous first-order functions of time. Then it is possible to solve the networks through a set of algebraic steps as described later. LIM has linear computational complexity and therefore it is highly scalable; consequently, it strongly reduces the computational effort required for the simulation of the network. A network has latency if each branch of the network contains an inductance and each node of the network provides a capacitive path to ground; if these values are not naturally present or if the present values are small and thus present latency much smaller than the time features of interest, additional capacitance or inductance can be added to increase latency (and hence the allowable time step).

As shown in Figure 2.3(a) any generic branch is composed of a series combination of a resistance, an inductance and a voltage source; applying KVL to the

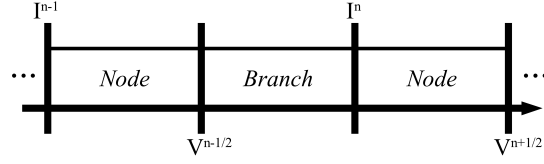


Figure 2.4 LIM Time Base

circuit of Figure 2.3(a), we can write the characteristic branch equation as:

$$V_i^{n+1/2} - V_j^{n+1/2} = L_{ij} \left(\frac{I_{ij}^{n+1} - I_{ij}^n}{\Delta t} \right) + R_{ij} I_{ij}^n + E_{ij}^{n+1/2} \quad (2.6)$$

From equation (2.6) it is possible to calculate the unknown branch current:

$$I_{ij}^{n+1} = I_{ij}^n + \frac{\Delta t}{L_{ij}} \left(V_i^{n+1/2} - V_j^{n+1/2} - R_{ij} I_{ij}^n + E_{ij}^{n+1/2} \right) \quad (2.7)$$

Equation (2.7) must be computed for all the branches of the network at each time step. As shown in Figure 2.3(b), each generic node is connected to ground via a parallel combination of a conductance, a capacitance, and a current source; applying KCL to the circuit of Figure 2.3(b) we can write the characteristic node equation as:

$$C_i \left(\frac{V_i^{n+1/2} - V_i^{n-1/2}}{\Delta t} \right) + G_i V_i^{n+1/2} - H_i^n = \sum_{j=1}^{M_i} I_{ik}^n \quad (2.8)$$

Where M_i is the number of branches connected to the node i . From equation (2.8) it is possible to calculate the unknown node voltage:

$$V_i^{n+1/2} = \frac{\frac{C_i V_i^{n-1/2}}{\Delta t} + H_i^n - \sum_{j=1}^{M_i} I_{ik}^n}{\frac{C_i}{\Delta t} + G_i} \quad (2.9)$$

Equation (2.9) is computed for all the nodes of the network at each half time step.

Using a leapfrog approach, the current through each branch and the voltage at each node can be updated alternately. The time is discretized and the current and voltage quantities are allocated in half time step; see Figure 2.4. The leapfrog structure of LIM integration is very important for power electronics converter modeling. It allows to represent ideal switching phenomena by linking nodes and

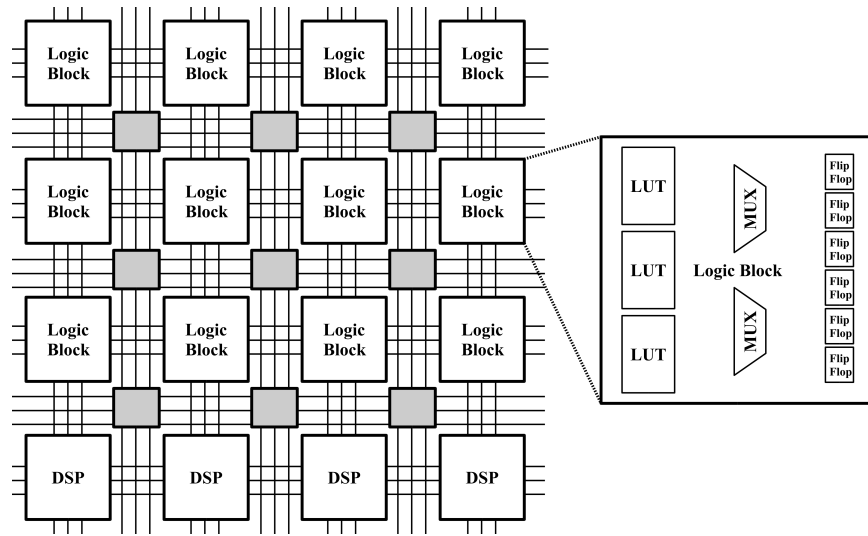


Figure 2.5 Diagram of Example FPGA

branches through their respective ideal voltage and current sources, with out introducing any additional delay in the integration.

2.3 FPGAs AND SIMULATION COMPUTATION IMPLEMENTATION

In recent years, Field Programmable Gate Arrays (FPGAs) have been widely used to perform real-time simulation of power systems. As seen in Figure 2.5, FPGAs are programmable logic devices consisting of an array of Look Up Tables (LUTs), Multiplexers (Mux), integer Digital Signal Processors (DSPs), and other digital logic elements which can be programmatically configured and linked together to create new digital circuits; examples of these circuits include signal switchers and converters, computational units, and even complete processors. These circuits can be created to operate independently from one another, enabling possibility of high parallelism of operations on a FPGA. Moreover, due to the hardware nature of FPGAs, operations performed by logic circuits on them have low-latency compared to performing same operations on a traditional processor or full DSPs. Integer operations, for instance, can be performed on FPGAs in mere nanoseconds in com-

binational logic fashion while similar operations on a CPU can take microseconds, requiring numerous clock cycles to compute result. From their high parallelism and low-latency, FPGAs are ideal for handling computations needed for real-time simulation.

Typically in software-based simulation, the use of floating-point data types, such as IEEE 754, are used to represent numerical values in models due to their high precision and dynamic range. However, computations with floating-point data typically require complex, high-latency, pipelined operations to handle the sophisticated data format. Such operations can require large amount of resources on a FPGA to implement, especially in using multiple computational units in parallel, and induce computational delay which can impede the ability to reach nanosecond time steps needed for real-time simulation of systems with high frequency dynamics. An alternative to floating-point data types on FPGA is fixed-point representation. Fixed-point represents numerical values with fractional elements where the decimal point is held fixed. Under fixed-point form, data bits before the decimal point represent integral portion of a value, while bits after the point represent the fractional part. Due to the simple and fixed nature of this data type, operations on fixed-point values can be performed as if the values are whole integers. As such, fixed-point operations can be easily instanced with simple combinational logic for integer arithmetic which can execute in a pipeline-less, dataflow manner. Fixed-point computational delay from this dataflow logic can depend almost solely on propagation delay of the comprised logic primitives. Since fixed-point arithmetic hardware is much simpler than floating-point hardware, the propagation delays can be kept low. along with low resource usage and delay, many FPGA platforms have built-in integer DSP slices or blocks which can be applied to accelerate operations and reduce delays of integer and fixed-point arithmetic. Despite the benefits of using fixed-point, the main downside to using this numerical representation is

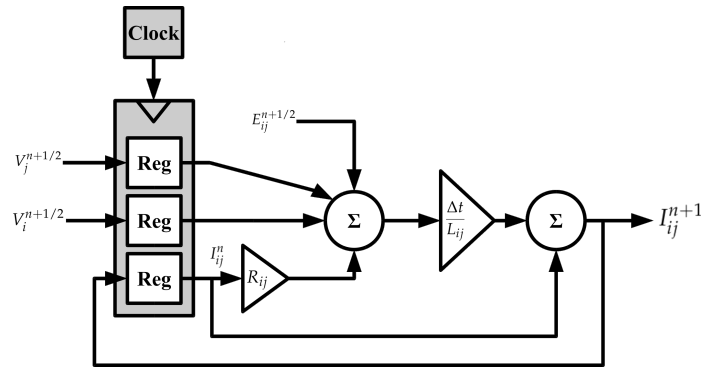


Figure 2.6 Hardware Implementation of Difference Equation for LIM Branch Current

limited numerical precision compared to floating-point, which can adversely affect numerical stability and accuracy. However, this limitation can be alleviated with careful selection of integral and fractional bit widths for fixed-point signals within a simulation, giving numerical accuracy comparable to use of floating-point arithmetic.

Most simulation methods that simulate non-linear behavior in a system typically use differential state equations in system models. To compute these equations on digital hardware such as FPGAs, these state equations need to be discretized with appropriate integration method, under given simulation time step, to become difference equations. These equations are composed of mere multiplication and addition operations which fit well on computational logic. For reduced computational resource usage and delay, explicit integration methods are suitable for creating difference equations to be executed on FPGA due to needing only to know past and present state to compute a solution; so long as time step is small enough to keep numerical stability. Since difference equations consider past states of a model from previous time steps in their design, these past states are stored in forms of memory to be accessed in present time step. On FPGAs, this memory can be embodied as registers which are instanced with simple flip-flops. Flip-flops are

state-based logic, so a digital clock is needed that drives the updates of the registers every time step. A complete FPGA implementation diagram of a difference equation for LIM branch current (2.7) is seen in Figure 2.6.

CHAPTER 3

LB-LMC REALIZATION ON FPGA

3.1 FPGA ENCAPSULATION

In this section, the encapsulation of the LB-LMC method elements for FPGA implementation is explained.

3.1.1 Component Entities

For each nonlinear component type used to model a system, a FPGA entity is developed. As input, these component entities take the system solution computed in a previous time step. Along with system solution, component entities can also take other input signals to control behavior of the entity, such as switch controller signals for a DC/AC converter component. At the beginning of each time step, the component entities sample and register their inputs. From these inputs and past internal states, the components perform their internal step for (2.3) and/or (2.4) and compute their source contributions.

An example component entity for a DC/AC converter (see Figure 3.5) is depicted in Figure 3.1. The DC/AC converter entity takes five inputs that are the DC bus and AC phase voltages on the terminals of the converter, and three switch control inputs to control the output phase modulation. Each time step, the component will register its past states and inputs from step k then use these to execute its internal step. The internal step for the converter involves handling the switching action of the converter through toggling bus capacitor voltages and filter inductor

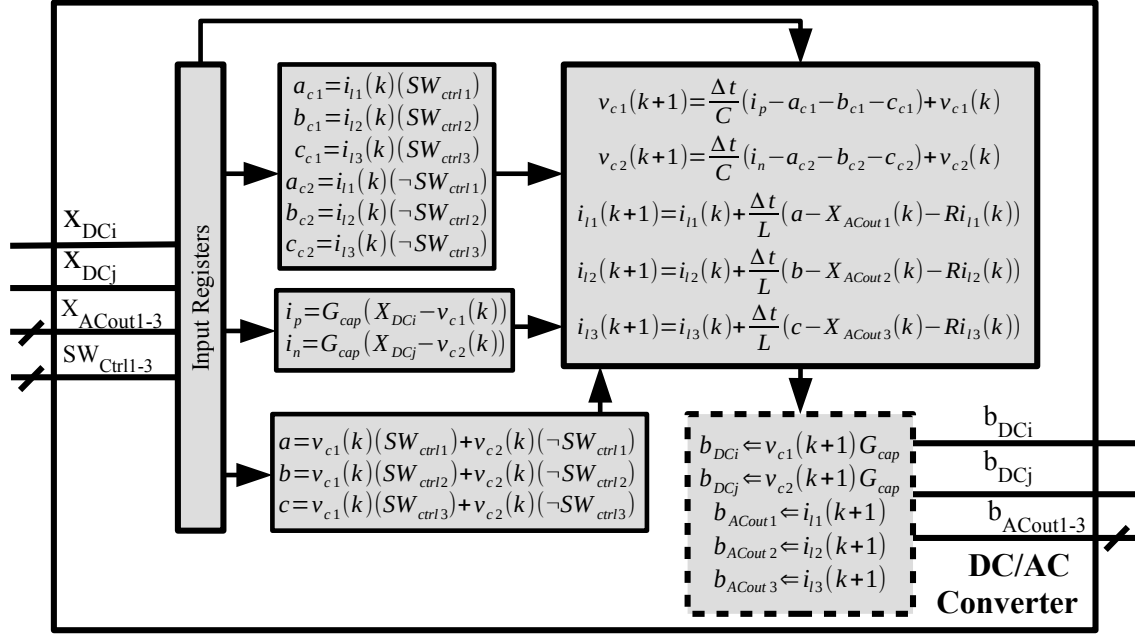


Figure 3.1 Example of DC/AC Converter Component Entity

currents ($a, b, c, a_{c1}, b_{c1}, c_{c1}, etc.$) and computing the said capacitor and inductors states for the current time step $k + 1$. The source contribution computational step (dashed block) computes the source currents for the bus capacitors and feeds these currents and the inductor currents out as the contribution output.

3.1.2 System Solver Entity

A dedicated system solver FPGA entity is created to compute the system solution. This solver entity takes as input the component source contributions and accumulates these contributions together to create the whole source vector b used to compute the system solution. The entity provides the system solution vector x as output which are fed back to component entities as input for the next time step execution.

Unlike the original LB-LMC method, the system solver entity does not use forward-backward substitution for system solution computation but instead uses

an inverted conductance matrix precomputed offline and multiple algebraic sum of product (SOP) expressions to find system solution. In this approach, the system solution is found by solving (2.5) for the vector x like in (3.1), where A is the inverted G conductance matrix ($A = G^{-1}$).

$$\begin{aligned} b &= f(v(k), i(k), I^n(k), V^n(k), k) \\ x(k+1) &= Ab \end{aligned} \quad (3.1)$$

This solution is computed by expanding the multiplication between A and b matrices into SOP expressions, like seen in (3.2), which are to be each computed individually from one another. Since the inverted conductance matrix is fixed, the A terms in the SOP expressions can be defined as constants in said expressions.

$$\begin{aligned} x = Ab \Rightarrow \begin{aligned} &A_{11}b_1 + A_{12}b_2 + \cdots + A_{1n}b_n \\ &A_{21}b_1 + A_{22}b_2 + \cdots + A_{2n}b_n \\ &\vdots \\ &A_{n1}b_1 + A_{n2}b_2 + \cdots + A_{nn}b_n \end{aligned} \end{aligned} \quad (3.2)$$

One main benefit of using this approach over forward-backward substitution is division operations are not required in calculations which tend to be computationally more expensive time-wise and use more FPGA resources compared to addition and multiplication operations. Moreover, this approach has only SOP expressions for the system that can be solved for system solution elements in parallel. A disadvantage to using this approach is that since the A matrix is precomputed offline and the SOP expressions are dependent solely on the system being modeled, the system solver entity and its expressions will have to be recreated or modified for each new system that is to be simulated.

3.2 SYSTEM SOLVER REALIZATION

In this section, we detail how the system solver can be designed to realize desired FPGA resource usage and computational latency.

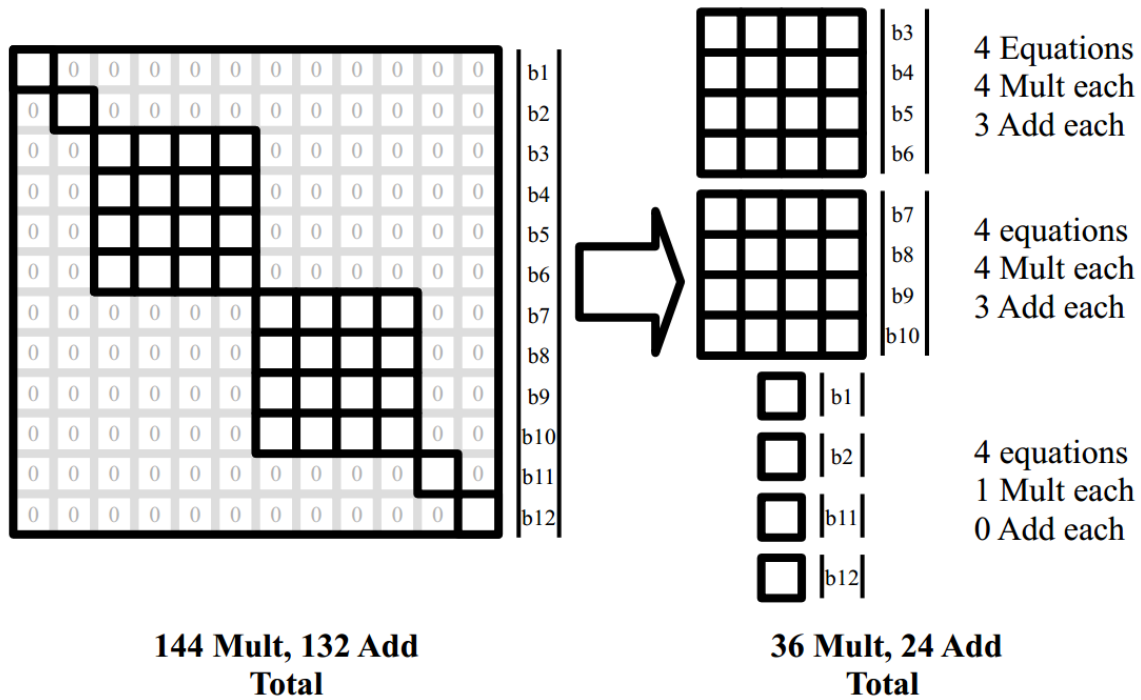


Figure 3.2 Separation of Subsystems

3.2.1 Subsystem Decomposition

Due to how the nonlinear behavior of components is moved to the source contribution computations from the conductance matrix in LB-LMC, it is possible to have multi-terminal components modeled as separate elements whose conductances are independent from one another. Then, the elements' behavior is coupled together via the component's internal step to properly model the whole component. From exploiting this separation of elements, the overall system model is expressed to contain independent subsystems which appear as independent diagonal blocks on the conductance matrix. A subsystem solver can be created from each diagonal block matrix and operated separately to compute a sub-vector of the solution. These subsystem solvers can be encapsulated into the top level system solver. The impact of using subsystem solvers is that the number of terms per system solution equation can be reduced substantially, lowering amount of FPGA hardware resources required.

An example of this subsystem separation for a 12-node system is shown in Figure 3.2. In this example, the system has two 4-node subsystem blocks and four 1-node blocks. If this system was solved without subsystem decomposition, 144 multiplications and 132 additions would be needed. However, with the decomposition, the operations are reduced to 36 multiplication and 24 additions, significantly reducing resources needed for the system solver. The shipboard power system models we present in this paper are expressed with a similar structure as this example.

3.2.2 System Solver Architecture

The system solver is implementable using two types of architecture: dataflow that solves solution equations in parallel within one pass, and multi-cycle which solves solution equations in multiple iterations within single time step. These architecture designs are explained below.

Dataflow Execution

In the dataflow implementation, the system solver solves all of its SOP solution equations in parallel, computing solutions without delay as component source contributions are produced. This approach allows solutions to be produced with minimal delay induced from requiring multiple clock cycles. This method requires that each solution equation has its own dedicated computational unit on the host FPGA, composed of smaller combinational operator units for multiply and add that are cascaded together in dataflow manner.

Multiple Cycle Execution

Another approach to implementing the system solver is to compute the system solution in multiple clock cycles per time step. The computation operations of

the system solver are broken up into units which are reused and iterated every clock cycle. Results from every iteration are compiled or accumulated to reach the system solution. The reuse of the same computational units every iteration allows reduction of FPGA resource usage for larger system models though at the expense of additional computational latency per time step.

An effective usage of multi-cycle execution is to iterate the solving of each subsystem block in a model. With such a setup, each subsystem block is solved each cycle of the system solver. If a model has sizable but few subsystem blocks, then using same subsystem solver and iterating it per subsystem can noticeably reduce resource usage while maintaining low enough clock latency for nanosecond-range time steps.

3.3 SIMULATION ENGINE COMPOSITION

This section provides explanation of how the entity encapsulations of the components and system solver are linked together on FPGA hardware to perform simulations.

To perform simulation of a system with the FPGA-adapted LB-LMC method, a simulation engine like seen in Figure 3.3 is composed, consisting of multiple component entities and one system solver entity tailored to the system simulated. In the engine, a component entity for each nonlinear component of the system is instanced and their source contribution outputs are linked to the appropriate inputs of the instanced system solver entity. The system solution output of the system solver is fed back to the component entities' inputs, the components taking solution elements that corresponds to their model terminals. If component entities require input from peripherals such as a switch controller, the appropriate FPGA elements are added to the design and linked to the requiring component entities. The updates of the components is performed with a digital clock on rising edge.

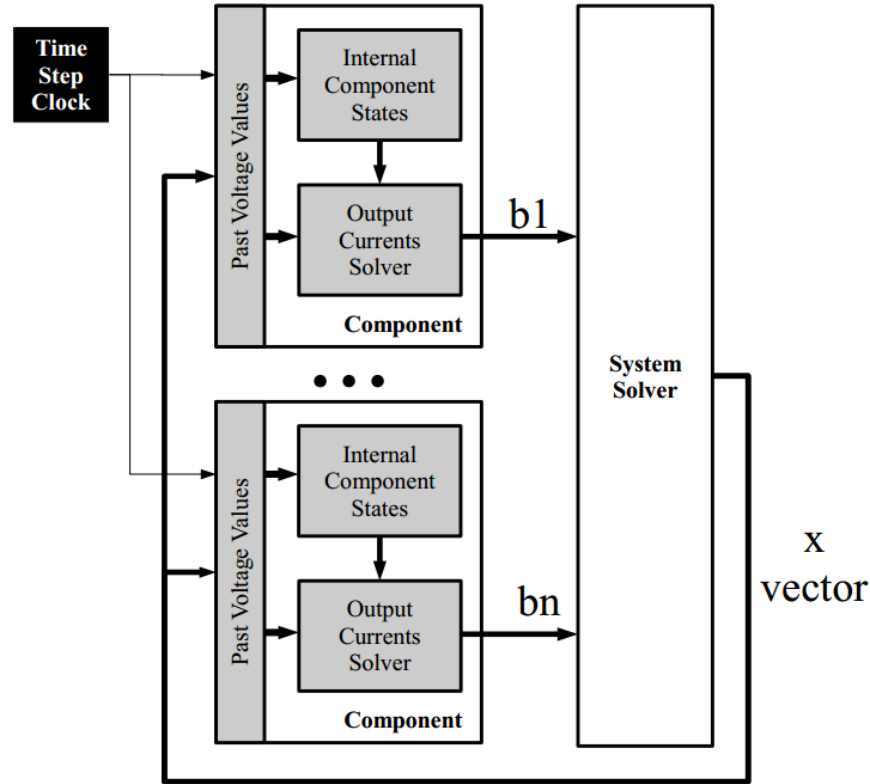


Figure 3.3 LB-LMC Simulation Engine

The execution scheduling of the simulation engine depends on whether the dataflow or multi-cycle system solver is used:

Single Pass with Dataflow System Solver

In use of the dataflow execution system solver, the simulation engine execution is performed in one pass, bounded to a system clock whose period is equal to the simulation time step. On the start of the time step, the component entities sample their inputs for the system solution from past time step and any peripheral inputs. Then, the components perform their computations. As source contributions' values are computed, the dataflow system solver will immediately compute the current time step system solution without wait. The choice of time step clock period is selected to be greater than the computational time needed by the simu-

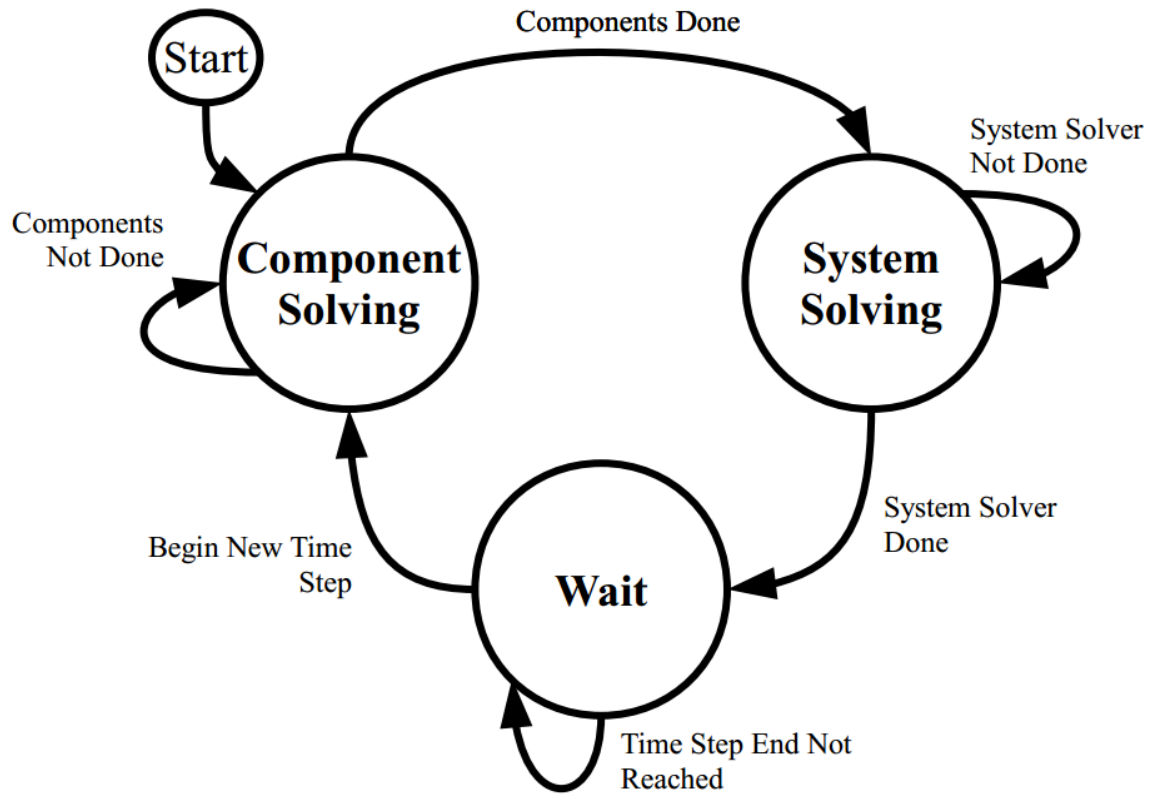


Figure 3.4 Finite State Machine for Multi-Cycle Simulation Engine

lation engine. The time step is set to be greater than the computational delay so as to ensure the simulation engine operates in stable manner.

Multiple Passes with Multi-cycle System Solver

For the simulation engine using the multi-cycle solver, the composition of the engine is similar to the single pass design, but multiple clock cycles are required to compute a system solution per time step period. In general, the component entities will likely need fewer clock cycles or none to compute their solutions compared to the multi-cycle system solver. Moreover, these component entities need to compute their solutions before the solver can begin. As such, a finite state machine is required to synchronize the execution of the component and system solver entities to one another and to the simulation time step. This finite state machine is

created to have the component entities solve their contributions first, and then allow the system solver to compute the system solution. Once the system solution is computed, the state machine has the engine wait until the beginning of the next time step period. This state machine driven operation is shown in Figure 3.4. The bounding of the entities' solution computation to each engine state is done through use of start input signals of each entity which is triggered by the state machine in each state.

3.4 FPGA IMPLEMENTATION

We discuss in this section the implementation of the LB-LMC simulation engines in regard to how computation execution is scheduled for parallelism and how numerical quantities are stored and processed.

For high scalability of performance of the LB-LMC method on FPGAs, the parallelism of FPGA hardware is exploited to accelerate computations. To utilize this high parallelism, all equation computations in component entities are expressed to be executed independently where possible, allocated to dedicated arithmetic units for each equation so that they can be solved in parallel. Furthermore, to avoid serial data paths in component entity computations, solution equations are expressed to avoid dependencies between one another where allowed by the component's model and solution integration method. Furthermore, all component entities are instanced with independent hardware.

Parallelism is also exploited in the system solver. For the dataflow solver, all system solution equations like seen in (3.2) are expressed to have dedicated arithmetic hardware provided to each one so they can be scheduled to run simultaneously. Moreover, the equations are implemented in dataflow manner, as discussed before, in the form of pure combinational logic composed of Lookup Table (LUT) and DSP slices which compute new solutions as soon as source contribution results

Table 3.1 DC/AC Converter Model Parameters

| V_{DC} | C_{DC_Bus} | L_{Filter} | C_{Filter} | R_{Load} |
|----------|---------------|--------------|--------------|------------|
| 12000 | 0.001 | 0.0001 | 1.0e-6 | 7.0 |

change. This execution manner allows solutions to be computed as soon as possible without having to wait for all source contributions to be computed by the component entities. In the multi-cycle system solver, the solution equations, though terms are looped, are also all implemented with separate hardware as well. Due to the repeated use of the arithmetic hardware in the multi-cycle solver for each solution equation during each time step, this hardware is pipelined to reduce number of cycles needed to reach a solution to be equal to number of terms per equation plus any cycles needed to fill the pipelines.

So that computational delays for the component entities and system solver is reduced and mostly dependent on the low propagation delays of the FPGA primitives, fixed-point arithmetic logic is used instead of floating-point logic for all calculations performed within.

3.5 TEST MODELS

In this section, the power electronic system models used to evaluate the LB-LMC FPGA simulation engine is discussed. Each model is of increasing size and complexity.

3.5.1 Three-Phase DC/AC Converter

A three-phase DC/AC converter, depicted in Figure 3.5, is modeled in LB-LMC method using parameters seen in Table 3.5. The converter operates with 12kV DC input. Switching frequency for the converter is 100kHz. The component entity of the converter model separates its internal elements into independent subsystems

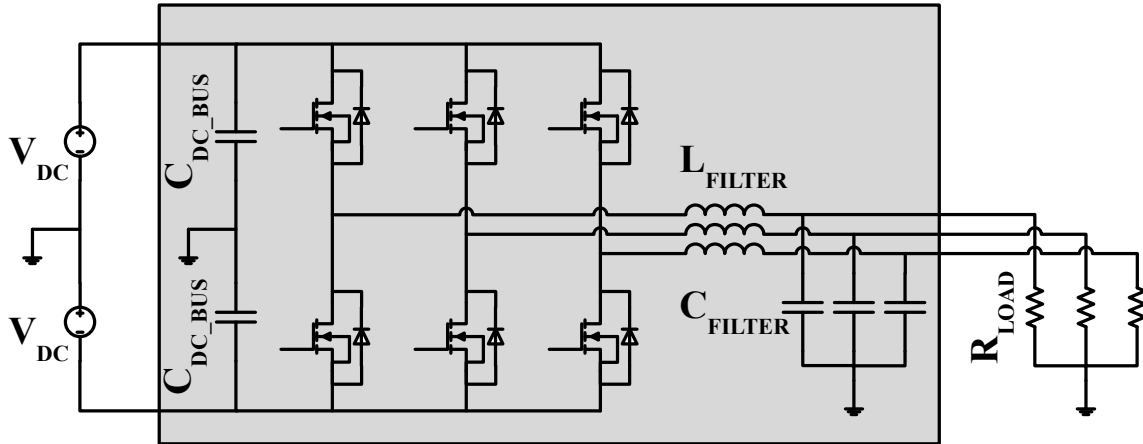


Figure 3.5 Three Phase DC/AC Converter

to allow subdividing the system solver into smaller block solvers, though the elements are coupled analytically through the internal step equations. Overall system has five node voltage solutions to solve, each associated with a 1-node subsystem block.

3.5.2 Single Bus Shipboard Power System

A single-bus power system found on ships, shown in Figure 3.6, is modeled using same converter model and parameters as the three-phase converter system, with other parameters chosen to have total system operate with 40MW load. This system contains three converters and uses a straight DC input source of 12kV. The overall system has 23 node voltage solutions to solve, and consists of two 7-node subsystem and nine 1-node subsystem blocks.

3.5.3 Dual Bus Shipboard Power System

A dual-bus shipboard power system, displayed in Figure 3.7, is similar to the single-bus system, but is composed of six DC/AC converters and two DC/DC converters. Parameters for this system is set for 40MW load and the DC/DC converters are set to output 12kV DC voltage onto bus lines. The overall system has

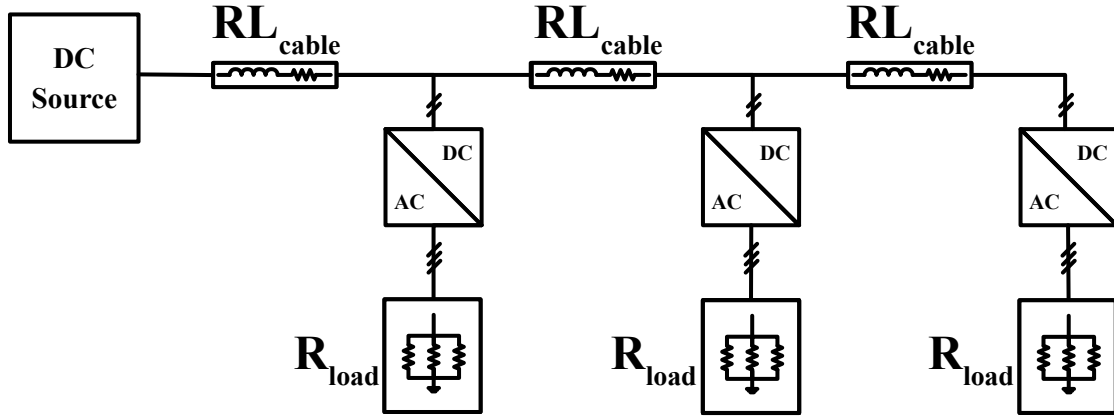


Figure 3.6 Single Bus Shipboard Power System

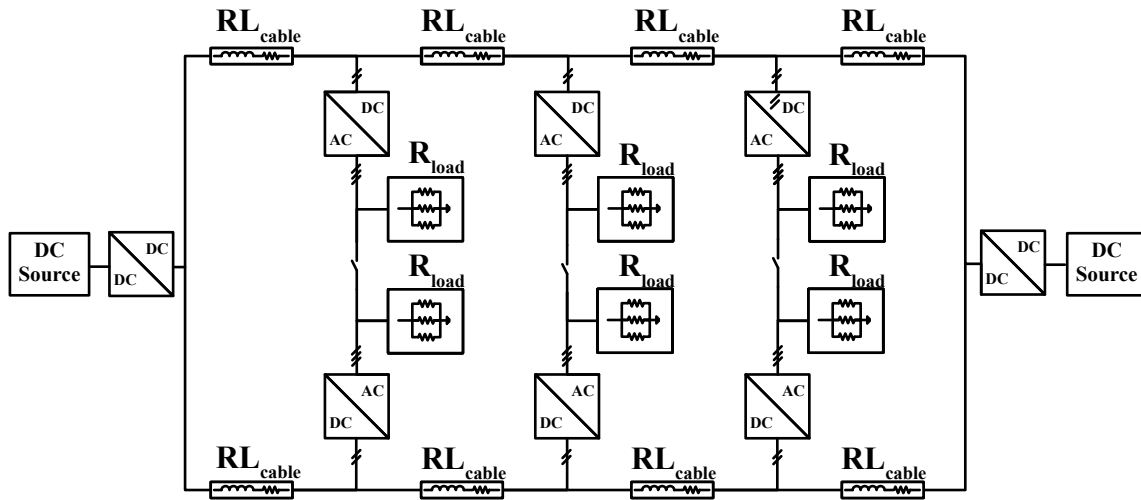


Figure 3.7 Dual Bus Shipboard Power System

54 nodes, and consists of two 16-node subsystem for the DC bus connections and twenty-two 1-node subsystem blocks for the loads and input DC sources.

3.6 IMPLEMENTATION RESULTS

In this section, we reveal results taken from separate LB-LMC FPGA simulation engines modeling in real-time the three power electronic systems discussed in Section 3.5. All models were run at 50ns time step, using the dataflow system solver. Resource usage and clock cycle latency of the dual-bus power system simulation

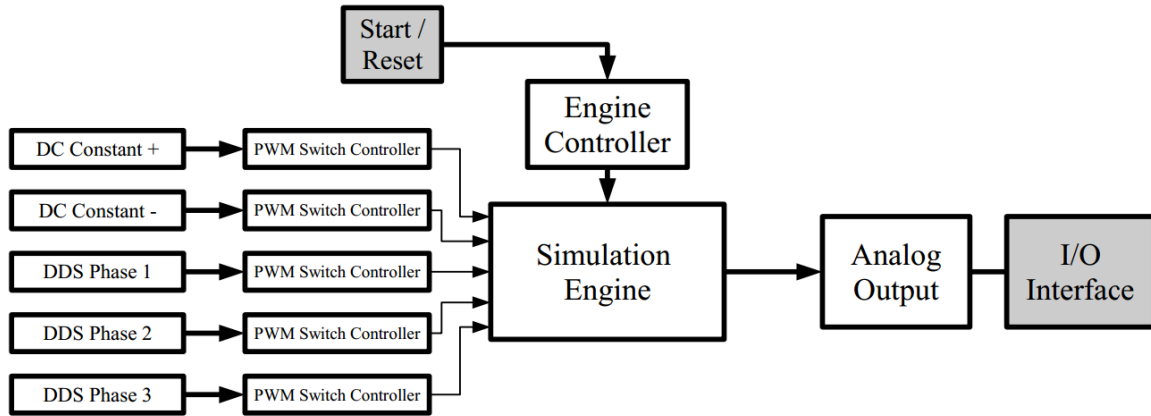


Figure 3.8 Top Level Design for Simulation Platform

engine using the multi-cycle system solver is also presented to show the change in results from moving to single-pass to multi-pass operation.

3.6.1 Setup

For all three models, the same top-level FPGA design was used, shown in Figure 3.8. The simulation engine was developed in C++ under Xilinx Vivado HLS 2015.4, and the complete top-level design was composed in standard Vivado using VHDL for the Xilinx Virtex-7 VC707 evaluation board; C++ code found in Appendix A. All numerical operations in the simulation engine were performed with fixed point logic defined with HLS `ap_fixed` library, using 72-bit width with 43-bit fractional precision. The engine controller seen in Figure 3.8 handles the start and reset of the simulation engine, as well as the wait state of the simulation engine's finite state machine when using a multi-cycle system solver. All models were run with open-loop switching control to minimize impact of correcting control action on simulation results.

Table 3.2 Model Error for LB-LMC

| | Three-Phase Inverter | Single-Bus Shipboard System | Dual-Bus Shipboard System |
|--------------------|-------------------------|-----------------------------------|---------------------------------|
| C++ LB-LMC (%) | 85.97e-06 | 0.0087 | 0.0141 |
| Traditional RC (%) | 2.234 | 1.459 | 1.1759 |

3.6.2 Simulation Accuracy and Error

To validate the accuracy of the results for each model, all system solution results, logged from the RTL-simulation of each model simulation engine design, is compared for error to a pure C++ implementation of the LB-LMC solver running at same time step length, using double precision floating point data type. Moreover, error comparison is made to a traditional resistive companion-based simulator running with 500ps time step. The error, shown in Table 3.6.2 was computed using two-norm (Euclidean) error equation, expressed here:

$$error\% = \frac{\|\hat{x} - x\|_2}{\|x\|_2} 100\% \quad (3.3)$$

, where \hat{x} is a matrix of all solutions taken over a 50ms simulation time period from the simulation engine and x is the matrix of all solutions from the reference solver in same time frame. As can be seen from the table, going to fixed point from double floating point data type has minimal impact on the the accuracy of the solver implementation, with error being less than one percent. Compared to the traditional RC solver, some accuracy is lost from applying LB-LMC solver. However, accuracy between solvers is still reasonably similar, with percentages of around 1-3%.

3.6.3 Real-Time Performance

The FPGA implementation is capable of simulating the presented power systems with a time step of 50ns in real-time. In comparison, the CPU/DSP software imple-

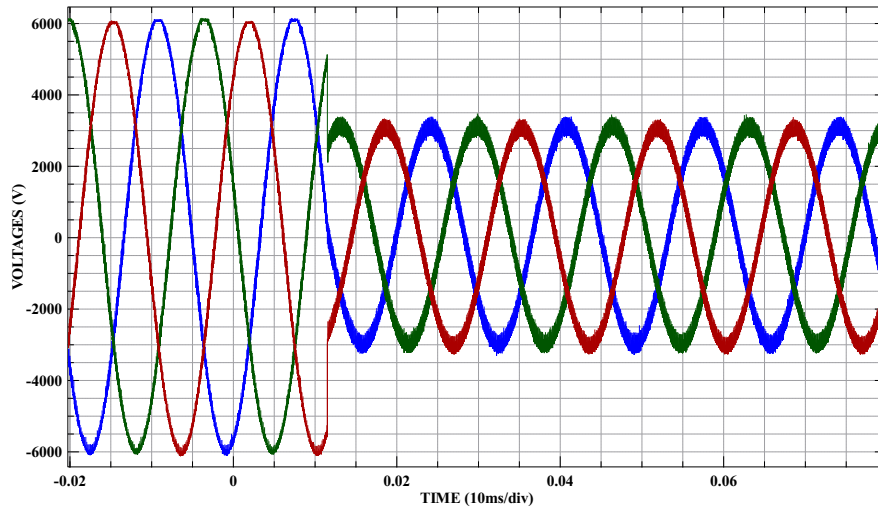


Figure 3.9 Single-Bus Power System Analog Output under LB-LMC

mentation of the LB-LMC method seen in [11] is only able to simulate in real-time at $15\mu s$ for a micro-grid power system similar to the single-bus shipboard system. The adaptation of the LB-LMC method from a software solution to a hardware solution has allowed for substantial decrease in computational time while still enabling real-time simulation of larger models.

3.6.4 Demonstration

The simulation engine designs of the two shipboard systems are loaded onto the VC707 FPGA board and analog output of each model was captured, via an oscilloscope, from their respective engine; results seen in Figures 3.9 and 3.10. For the single-bus system model results, three AC output phases from one of the DC/AC converters is shown. The dual-bus system results displays two of the output phases and the positive and negative DC bus line voltages. The results for the single-bus system were captured while switch control for the DC/AC converters was set to reduce phase output voltage by half suddenly. Similarly, the dual-bus system results were captured while the switch control of the DC/DC converters

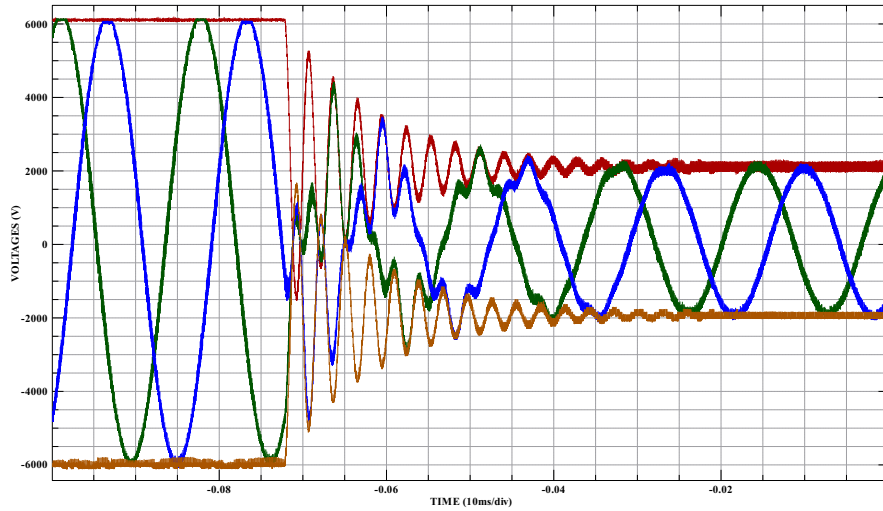


Figure 3.10 Dual-Bus Power System Analog Output under LB-LMC

powering the system was set to reduce bus voltage to simulate sudden drop in DC/DC converter voltages. Ringing in the dual-bus system voltages is consistent with traditional Resistive Companion Method version of said system, and is expected due to operating without closed-loop control to correct for the oscillations, as well as the sudden change in voltage by the control.

3.6.5 Multi-cycle System Solver Resource Usage

To evaluate impact on resource usage from using a multi-cycle system solver with subsystem iteration, the system solver for the dual-bus shipboard system was implemented in Vivado with the dataflow design and the multi-cycle design for a 50ns clock cycle, where the dataflow is expected to compute its solution before 50ns while the multi-cycle design is clocked every 50ns. Each version of the solver was implemented separate from the top-level design so that the resource usage reports shown the system solvers' usage only. The multi-cycle version was designed to use same subsystem solver unit for the two subsystems in the shipboard system and compute all solutions and be prepared to receive new source contribution in-

Table 3.3 Resource Usage for Multi-cycle System Solver

| | Dataflow | Multi-Cycle |
|--------|-------------|-------------|
| Cycles | 0 | 2 |
| DSP | 724 (26%) | 466 (17%) |
| LUT | 54172 (18%) | 36349 (12%) |
| FF | 0 (0%) | 3830 (0.6%) |

puts within two cycles; effectively doubling the feasible time step. Both versions solved the 1-node subsystems all in parallel to the subsystem computations. The resource usage of the two system solver architectures and their usage percentage on the Virtex-7 FPGA is shown in Table 3.3. As can be seen from the results, using the multi-cycle design reduced DSP and LUT usage of the total system solver by approximately 33-36% compared to the dataflow design while still allowing the simulation engine to perform with a reasonable 100ns time step. Though not an one-to-one tradeoff between latency and resource usage, this resource reduction is significant enough to highlight that this multi-cycle approach can enable simulation engines of large models to potentially fit on a given FPGA where resource usage of a dataflow solver may not allow. Flip-flop usage went up from needing to maintain memory for the iterations of the multi-cycle architecture, but usage percentage on the Virtex-7 is insignificant at below one percent.

CHAPTER 4

LIM REALIZATION ON FPGA

In this chapter, the realization of Latency Insertion Method on FPGA is presented. First, how LIM components are encapsulated into FPGA entities is discussed, followed by how these entities are linked together to compose a simulation solver engine. Then, the handling of switching action of switching converters in LIM models are explained. Finally, implementation details are discussed and real results from real-time simulation with implemented LIM engines are given.

4.1 FPGA ENCAPSULATION

LIM maps well to FPGA architecture due to the high parallelizability of branch and node models, and to the natural expression of the model equations as difference equations which align with the discrete hardware of FPGA devices. To implement a LIM-modeled circuit in a FPGA design, a structural entity is created for both the branch model and the node model; see Figure 4.1. For the branch model, its entity takes as input signals node voltages V_i^{n+1} and V_j^{n+1} , and dependent voltage source E_{ij}^{n+1} , and outputs the branch current I_{ij}^{n+1} . The entity for the node model takes as input the branch current sum $\sum_{k=1}^{M_i} I_{ik}^n$ (as single signal) and dependent current source H_i^n , and outputs node voltage $V_i^{n+1/2}$. Parameterizing these entities for particular circuit branches and nodes (setting L, R, and C), the parameters of the entities can be set through generics which configure them during FPGA synthesis of simulated models' design. In each LIM entity design, their respective model equations (2.7)(2.9) are implemented as signed fixed-point computational

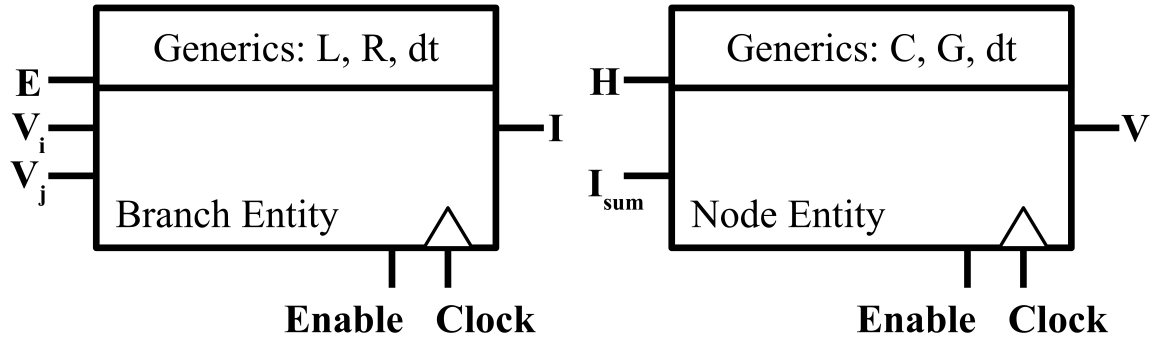


Figure 4.1 FPGA RTL Entities for LIM Models

logic synthesized from the difference forms of said equations. These equations are updated once every full time step, using registers to retain past time step states ($I_{ij}^n, V_i^{n-1/2}$) and entity output for next half time step entity input ($I_{ij}^{n+1}, V_i^{n+1/2}$).

4.2 SIMULATION ENGINE COMPOSITION

To compose a simulation computation engine FPGA design that will simulate a modeled circuit, branch entity output current signals are connected to input signal ports of the node entities, and output voltage signals are connected to input ports of the branch entities, corresponding to topology of modeled circuit in question; like seen in Figure 4.2. If multiple branch currents are to feed into a node, they are summed together and the result is given to corresponding node. Driving the updates of the LIM model entities, a digital clock is fed into all entities which clocks the internal state and output registers. Since a time step is divided into two halves, one for branches and the other for nodes, the time step clock has a period half that of the desired time step length (twice as fast) to have one clock period per half time step. So that branches and nodes are updated in leapfrog fashion, a simple finite state machine of two states is used to decide when branches and nodes can update through start signals for each.

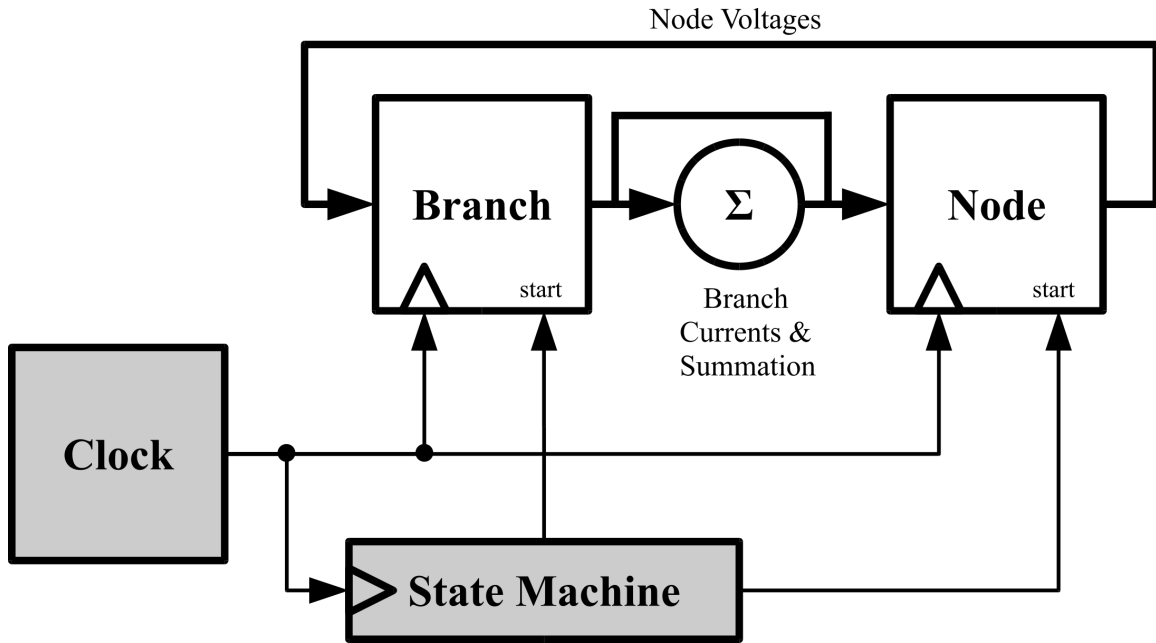


Figure 4.2 LIM Simulation Engine FPGA Design

4.3 SWITCHING POWER CONVERTERS IN LIM

In general, most circuits with sufficient reactive latency can be simulated with LIM. This fact holds true for switching power converters which commonly contain capacitive and inductive elements. In such circuits, the arrangements of the latency components often align with LIM branch and node models. Application of this alignment to model switching converters is demonstrated in the following examples for a buck converter and three-phase inverter.

4.3.1 Buck Converter

Take for instance the ideal buck converter shown in Figure 4.3. In the buck converter, the output filtering capacitor and load resistance are mappable to a LIM node, the inductor is mappable to a LIM branch, and the voltage source input and input capacitor are mappable to another LIM node after the voltage source has been transformed into a current source with Norton's transformation. This map-

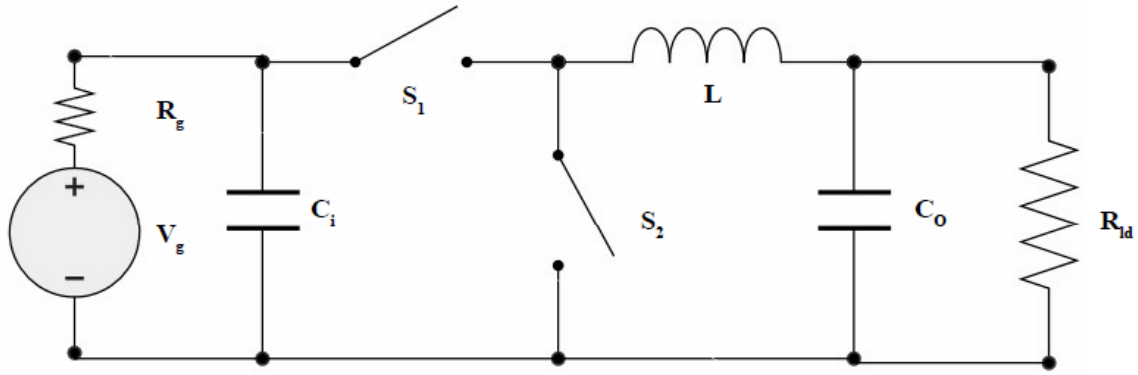


Figure 4.3 Buck Converter

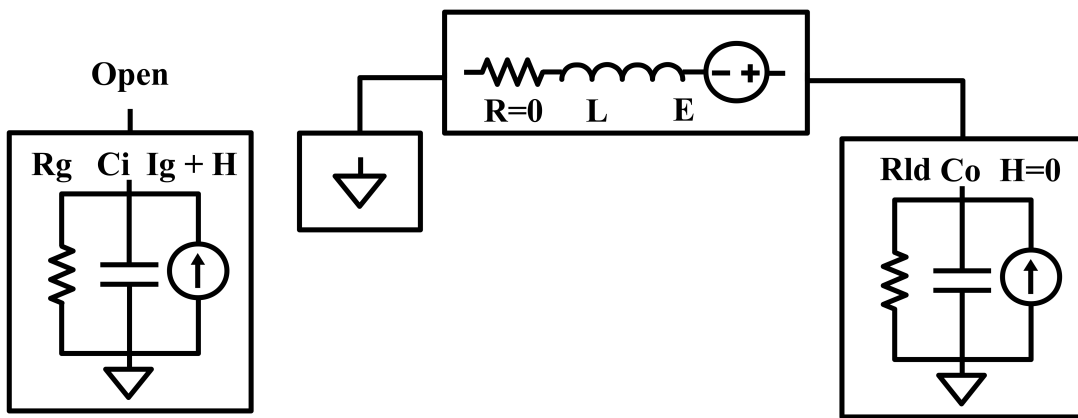


Figure 4.4 Buck Converter LIM Model

ping to LIM components is shown in Figure 4.4. The question arises on how to handle the switching action of the buck converter with LIM. As seen in previous discussion on LIM, branch and node models contain respectively a voltage source E and a current source H which can be arbitrarily altered during simulation. Using these model sources, the switching action can be handled by altering the values of H and E in LIM component models in sync with the switching states of a simulated converter. Applying this idea to the topology of the buck converter with continuous mode switching like seen in Figure 4.5, one can equate during switch-on state the E term of the inductor branch to the input voltage across the input capacitor node, and equate the H term of the input capacitor node to the inductor branch

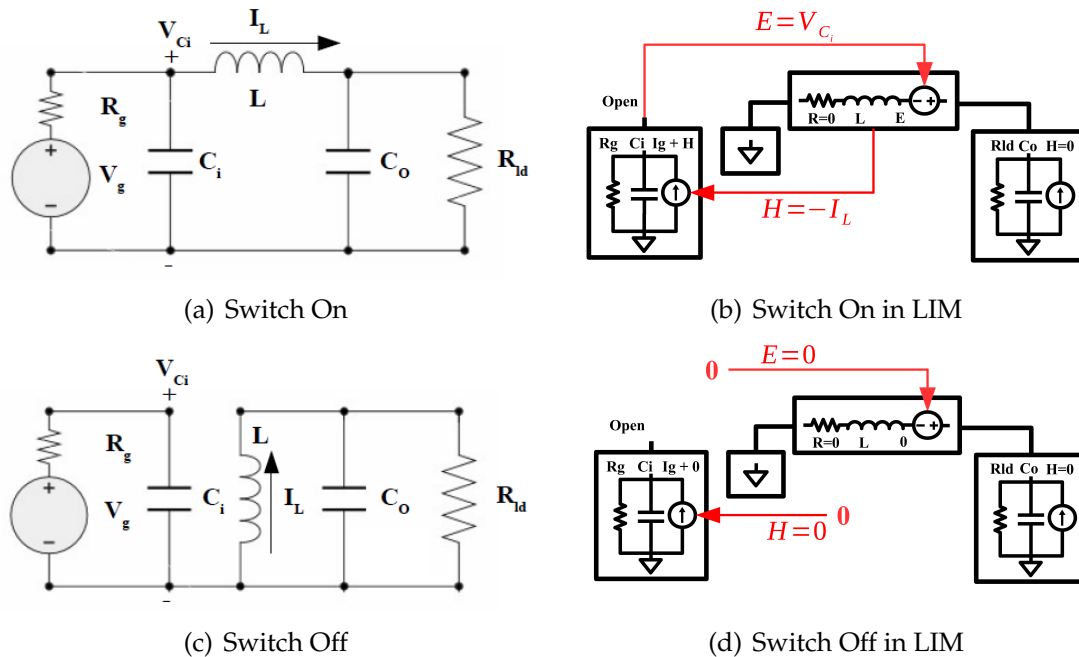


Figure 4.5 Buck Converter Switching Action with LIM Model

current. During the off state of this converter, both H and E are set to zero. By altering H and E terms according to a switching control signal, the switching action of the converter using LIM is simulated. Other converters, such as the three phase inverter discussed below, can also be simulated with LIM in similar approach. For switching behavior in general, H and E terms of switching power converter LIM models are typically functions of the LIM branch currents and node voltages, with functions being selected based on switching state of converter.

4.3.2 Three-Phase DC/AC Converter

A three-phase DC-AC converter can be modeled following an approach very similar to the one adopted for the buck converter. As can be seen from the converter's topology as an inverter, seen in Figure 4.6, the inductors can be mapped to LIM branch models each, the DC bus capacitance can be modeled as LIM nodes, along with the output capacitor filter and resistive load. This mapping of the DC/AC

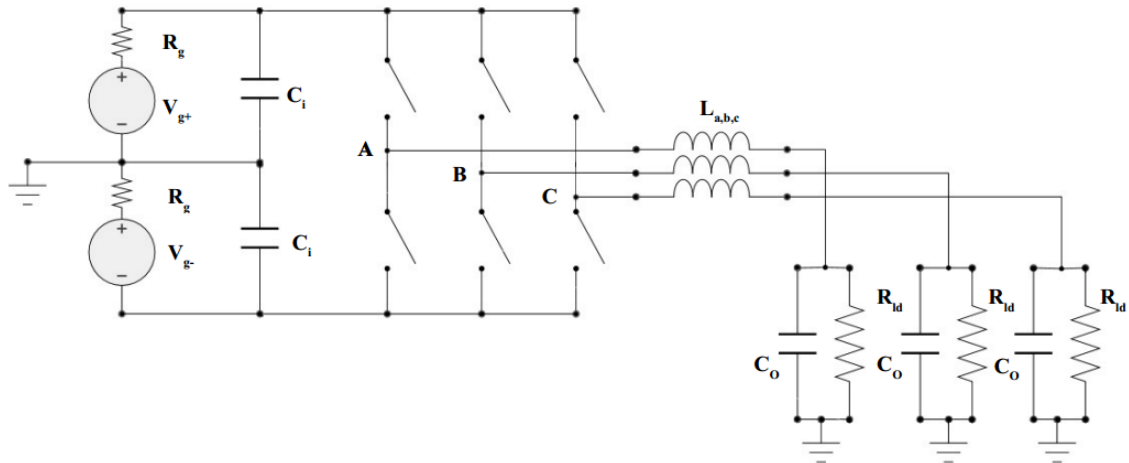


Figure 4.6 Three-Phase AC/DC Converter as Inverter

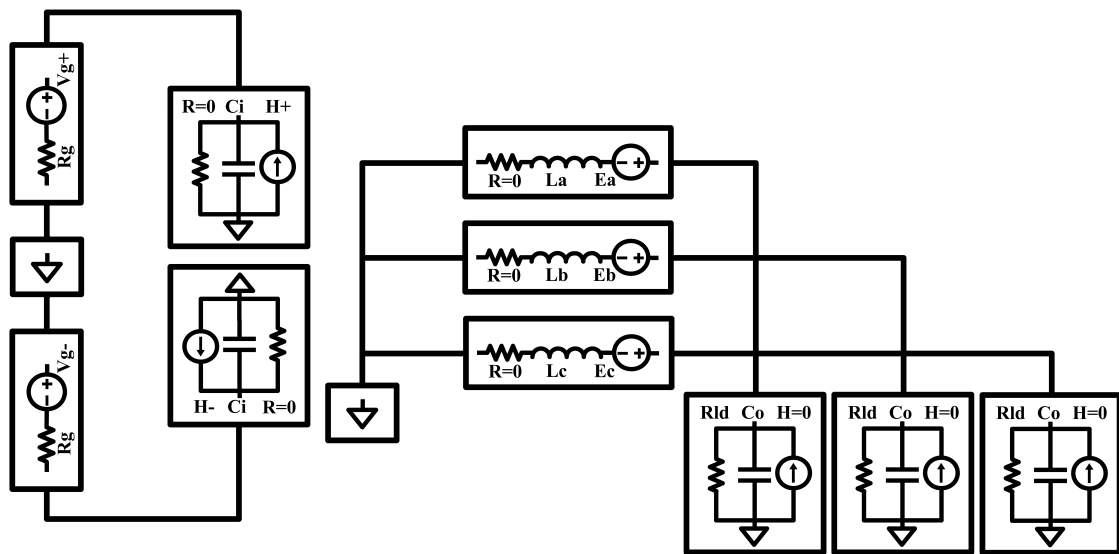


Figure 4.7 Three-Phase Inverter LIM Model

converter to LIM is seen in Figure 4.7. In this case, since the input voltage sources with series resistance is held as constant and has no capacitive or inductive elements, these sources can be treated as purely resistive branches without latency, modeled by:

$$I_g^{n+1} = \frac{1}{R_g} (V_g - V_j^{n+1/2}) \quad (4.1)$$

which can be used as LIM-compatible branch current quantity.

To handle the switching action of the three-phase converter, The H terms for the input node models can be set as functions of the three inductor branch currents, like so:

$$\begin{aligned} H_+ &= -I_a s_a - I_b s_b - I_c s_c \\ H_- &= -I_a \bar{s}_a - I_b \bar{s}_b - I_c \bar{s}_c \end{aligned} \quad (4.2)$$

where s_a through s_c and their inversions are the three-phase converter's modulating switch control signals per phases $a-c$, either of value zero or one. Then, for the E terms of the branch models, their functions can be declared as:

$$\begin{aligned} E_a &= V_+ s_a + V_- \bar{s}_a \\ E_b &= V_+ s_b + V_- \bar{s}_b \\ E_c &= V_+ s_c + V_- \bar{s}_c \end{aligned} \quad (4.3)$$

where V_+ and V_- are the voltages of the DC bus capacitance nodes, respectively.

To model switching action with deadband interval for this converter, extra functions are applied for H and E when both switches are off (zero). In this case, the functions for one of the converter legs is:

$$H'_+ = \begin{cases} 0.0 & I_a > 0.0 \\ +I_a & I_a \leq 0.0 \end{cases} \quad (4.4)$$

$$H'_- = \begin{cases} 0.0 & I_a \leq 0.0 \\ -I_a & I_a > 0.0 \end{cases} \quad (4.5)$$

$$E_a = \begin{cases} V_- & I_a > 0.0 \\ V_+ & I_a < 0.0 \\ V_a & I_a = 0.0 \end{cases} \quad (4.6)$$

where V_a is the output phase voltage. The H'_+ from each converter leg are added to get H_+ for complete converter during deadband interval; the same for H_- . These

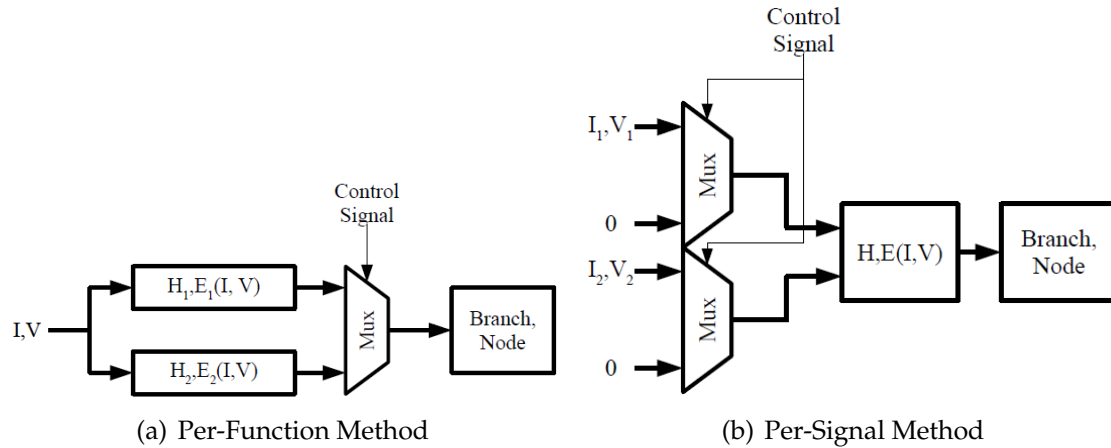


Figure 4.8 Handling Switching Action in LIM Simulation Engine

equations assume that the converter switches have anti-parallel diodes across them which conduct appropriately during deadband interval.

4.3.3 Converter Switching Behavior Handling on FPGA

Since H and E terms of branches and nodes of switching circuits are generally functions of branch currents and node voltages, switching behavior can be implemented by feeding results of functions of these current or voltage signals into a multiplexer whose output feeds into respective H or E input of a LIM entity, as shown in Figure 4.8(a). Based on the switch state of the converter driven by a switch control signal, whether continuous or discontinuous mode, appropriate function can be selected via the multiplexer. Seen in Figure 4.8(b), another way to handle switching behavior is to have branch current and node voltage signals switched on or off as input to the H and E functions with multiplexers, based on the switching signal. In any case, the H and E functions are implemented as simple dataflow computational expressions which are expected to produce stable output within the half time step of entity that is recipient of said functions' results. Selection of handling method is largely dependent on the converter model to be simulated with LIM.

4.4 FPGA IMPLEMENTATION

This section presents the implementation of the LIM simulation engine in regard to how computation execution is scheduled for parallelism and how numerical quantities are stored and processed.

Similar to LB-LMC, the parallelism of FPGAs is exploited by having the equations of the branch and node entities expressed to be independently from one another through using dedicated computational elements for each equation. Each entity is designed to operate separately and in parallel to its own type (branch or node) and only depend on results provided from prior half time steps as input. The same setup also applies to computational units needed to handle switching action for both branches and nodes, and branch current summation for node entities. All operations performed in each half time step update are implemented to finish in one pass through use of dataflow computational design, requiring two complete passes for a full time step. For same reasons as in LB-LMC FPGA implementation, discussed in Section 3.4, fixed point arithmetic is used for all calculations.

4.5 IMPLEMENTATION RESULTS

4.5.1 Setup

To demonstrate implementation of LIM models of power systems, the test models found in Section 3.5 were re-implemented with the LIM FPGA simulation engine, using same top-level design as seen in Figure 3.8, with the LB-LMC simulation engine replaced with the LIM one. Again, the same Xilinx VC707 evaluation board was used in the setup. The simulation engines were developed in C++ with Xilinx Vivado VHLS 2015.4 and used 64-bit signed fixed point data types with 35 fractional bits; C++ code found in Appendix B. All engines ran at 40ns time step, using a 20ns clock source.

Table 4.1 Model Error for LIM

| | Three-Phase Inverter | Single-Bus Shipboard System | Dual-Bus Shipboard System |
|--------------------|-------------------------|-----------------------------------|---------------------------------|
| C++ LIM (%) | 0.0266 | 0.0488 | 0.0551 |
| Traditional RC (%) | 1.7394 | 1.5036 | 1.4523 |

4.5.2 Simulation Accuracy and Error

To validate the accuracy of the LIM FPGA simulation engine for each of the test models, both branch current and node voltage results were logged from RTL-simulation of each model engine design. Then, the results were compared for error to offline C++ implementation of the LIM solver running at same time step with double precision floating type and afterwards compared to traditional resistive companion based simulator running with 400ps time step. Error was computed using (3.3). Results were taken over a 50ms simulation time period after results have reached steady state for the models. The computed error results are shown in Table 4.1. Despite going to fixed point type which typically has lower precision than floating point representation, the FPGA implementation of LIM had low error well below one percent compared to the C++ implementation with double precision float. In comparison to the traditional RC Solver, error was between 1.45 to 1.74 percent, which though not ideal, is reasonable in approximating the given models analytically.

4.5.3 Demonstration

As was done for the LB-LMC simulation engine, the engine designs for the shipboard systems were loaded onto the Xilinx VC707 FPGA and analog output from the board was logged, as seen in Figures 4.9 and 4.10. The output phases of one of the converters for the single bus system were captured while the switch control suddenly changed output voltage to higher level. For the dual-bus system, the DC

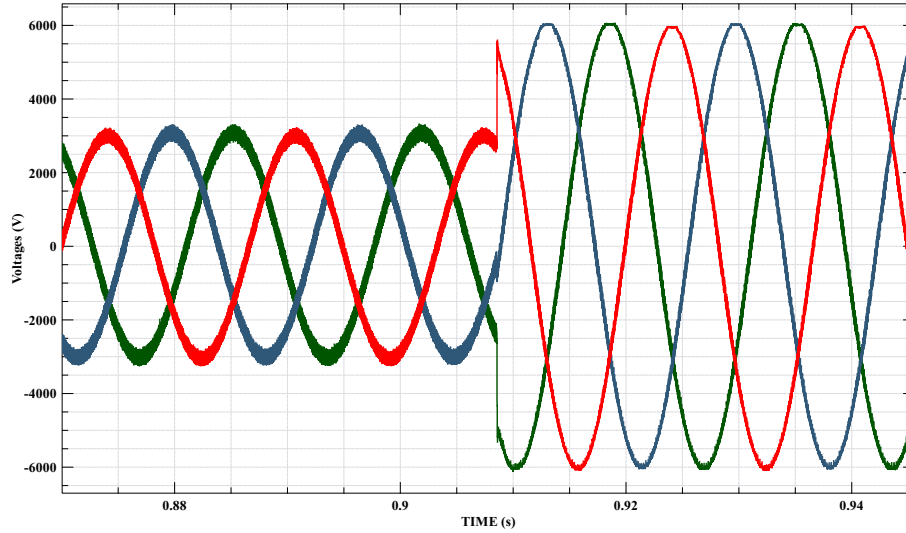


Figure 4.9 Analog Output for Single-Bus Power System under LIM Engine

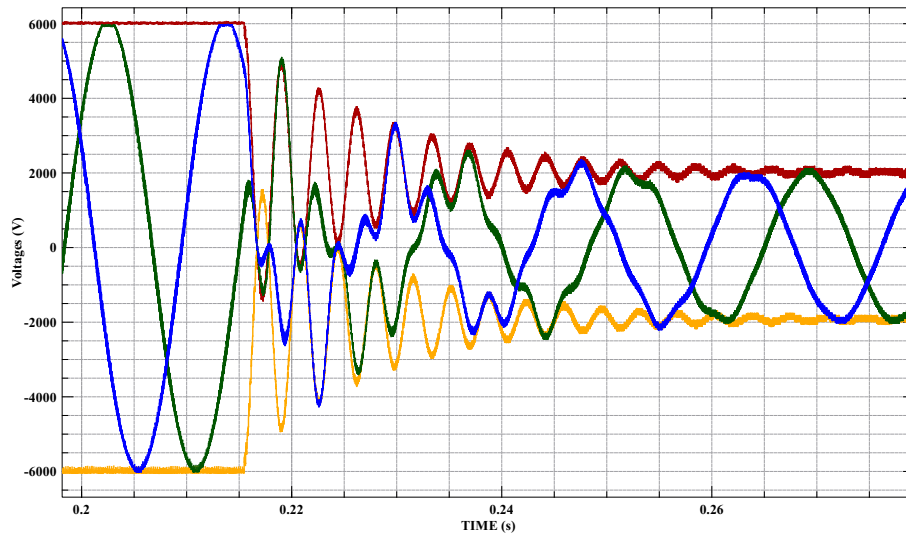


Figure 4.10 Analog Output for Dual-Bus Power System under LIM Engine

bus voltages and two of the output phases from one of the converters, the same as for the LB-LMC implementation, were taken during condition that switch control induced sudden change in output voltages. Comparing to results seen in Section 3.6.4, the results taken from the LIM simulation engines are highly similar to LB-LMC versions of same models, as expected. This relation suggests that the two

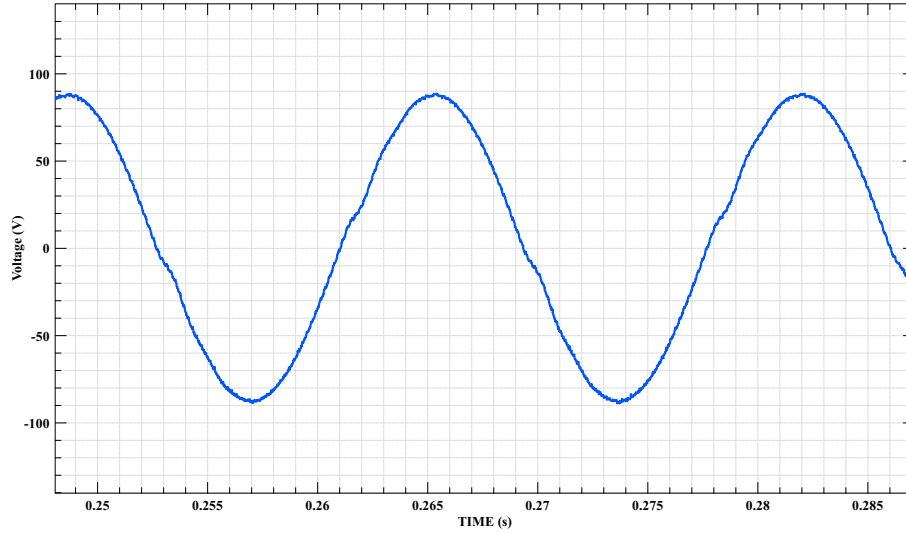


Figure 4.11 Deadband Interval Distortion Result

simulation methods, though different in their implementation and structure, are analytically equivalent within reasonable boundaries, at least for these test models.

To demonstrate deadband interval in the switching action, a tuned, three-phase DC/AC converter simulation engine with induction load in the converter model was created, using suboptimal deadband time of 260ns for 100kHz switching frequency. One of the phases for the converter taken in real-time, showing visible distortion from deadband interval, is shown in Figure 4.11.

CHAPTER 5

SCALABILITY ANALYSIS

One of the important aspects to choosing a simulation method for FPGA implementation is how the method scales on such hardware as the size and complexity of the simulated system grows. One element of scalability is computational delay which affects the size of time step usable. Should a simulation method require quadratic or even linear scaling of delay as the model grows, the time step achievable for large systems may become too great to precisely capture model behavior in real-time during simulation. As such, it is desirable to have computational delay scale sublinearly or stay constant as a model grows in size. Another element is amount of resources required to realize the computations. To achieve low computational delay in the nanosecond range, it is required to exploit parallelism on FPGAs to maximize number of computations in a given time. This parallelism is achieved by giving each computation of an equation or expression in a system model dedicated resources on the given FPGA. Therefore, as a model grows in size, so does the resources needed to simulate the model. Since all FPGAs have finite amount of resources to give for a simulation engine of a given method, understanding how resources scales with model size is important to ensure larger system models can fit on a chosen FPGA device. In this chapter, the computation delay and resource usage of LB-LMC and LIM are analyzed at element level, and the methods are compared within this regard using real-world results taken from a model of increasing size.

5.1 LB-LMC

This section discusses the scalability of the FPGA implementation of the LB-LMC solver as model size increases, in terms of achievable time step (computation delay), clock cycle latency, and FPGA resource usage.

5.1.1 Components

The number of operations required to compute the internal states and source contributions of a component is largely dependent on the component model and integration method used. However, the total number of operations required for a collection of components of same model and type will scale linearly as more components of same type are instanced in a simulation engine. This linear scaling of operations also applies to resource usage as each operation of same type uses similar amount of resources. Though resource usage will increase linearly with number of components, the computational delay for all components of same type to perform their operations will stay constant due to the parallel operation of said components.

5.1.2 Dataflow System Solver

As the size of a modeled, independent system or subsystem grows to n solutions, the number of operations required for the solver grows by an order of 2, with number of multiplications needed being n^2 , and additions being $n(n - 1)$. If each operation type (multiplication or addition) is mapped to unchanging FPGA resources without any FPGA synthesis optimizations, the amount of resources needed for the dataflow will also grow by an order of 2 as well. Due to this growth of resources, the system solver can act as a bottleneck that determines how large of a model and its simulation engine can fit on a given FPGA device. To reduce number of operations and FPGA resources in the dataflow system solver, the modeled

system is broken up into subsystems where possible and each subsystem is given its own solver with reduced size n .

The computation delay of the dataflow system solver will grow sublinearly as a model size increases due to the multiplication and addition operations performed in parallel, dataflow manner on FPGA hardware. This scaling is unlike a traditional CPU or DSP whose computational time or delay for the solving of these system equations will grow with an order of 2 as the number of solutions increases, due to performing all operations sequentially.

5.1.3 Multi-cycle System Solver

The number of operations implemented in hardware of the multi-cycle system solver is inversely proportional to the number of iterations selected for the solver to compute a solution. Resource usage will scale similarly, though extra resources are required to enable multi-iteration computation and pipelining. Computational time of the system solver is a function of cycles needed for the solver to reach solution, where the time is a product of the number of cycles, including extra cycles for pipeline priming, and the clock period used.

5.1.4 Simulation Engine Time Step and Computation Delay

The time step usable for the simulation engine is dependent on the computational delay and latency of the components and system solver. With the dataflow system solver, the time step must be greater than the sum of computational delay required for the slowest component entity type and the delay needed for the system solver to have all solutions computed and stabilized; this sum being the total computational delay of the simulation engine:

$$\Delta t > t_{solver} + t_{comp_delay} \quad (5.1)$$

For larger system models, it is expected that the simulation engine computational delay will be dominated by the system solver delay as component model entities' delays do not grow with system size and expected to typically be small in computational complexity. To greatly reduce system solver delay, and reduce time step, subsystem decomposition can be used within the system solver as noted before.

In the case of using a multi-cycle system solver, the system solver will again greatly influence the time step for the simulation engine due the solver's need for multiple cycle latency needed to reach the system solution each time step. The computation time of the simulation engine will be the number of cycles needed for system solver to reach solution times the clock period used to clock the solver, plus the delay needed for the slowest type of component entities to perform their operations. From this relation, the time step will have to be:

$$\Delta t > n_{sol_cycles} t_{clk} + t_{comp_delay} \quad (5.2)$$

Reduction of multi-cycle system solver latency, and in turn the time step, can be achieved through reducing the number of cycles needed to compute the solution through performing more system solution equation operations per cycle, or to an lesser effect, reduce the clock period. In either case, the tradeoff is higher usage of FPGA resources.

5.2 LIM

This section discusses the scalability of the FPGA implementation of the LIM solver as model size increases, in terms of achievable time step (computation delay), clock cycle latency, and FPGA resource usage.

5.2.1 Entities

Due to the fixed nature of the component entities in LIM, the number of operations within a branch and a node component will stay constant, regardless of the system model and its size. Therefore, the total number of operations needed for a given number of branches and nodes in a model grows linearly with the model in question. Since resources realize these operations, they will increase at same scale as said operations. Though resource usage grows linearly, computational delays for both branch and node entities shall stay relatively constant due to entities of same type all updated in parallel.

5.2.2 Simulation Engine Time Step and Computation Delay

Due to the leapfrog approach used to handle the simulation flow of the LIM engine, and using the same clock period for branch updates and node updates, the achievable time step for a given system model will always be greater than or equal to twice the said clock period, expressed as:

$$\Delta t \geq 2t_{clk} \quad (5.3)$$

This clock period t_{clk} is a function of how long the engine takes to compute the longest half time step update period, whether for branch updates or node updates. The computation time for the update periods is influenced by switching action computations performed under either component update time for converter simulation and by computational time needed to sum branch currents together for a given node component during node update period; on top of computational time for branches and nodes themselves. For branch updates, the compute time will be:

$$t_{branch} = t_{switch_compute} + t_{update} \quad (5.4)$$

and for the node updates:

$$t_{node} = t_{switch\|sum_compute} + t_{update} \quad (5.5)$$

, where $t_{switch||sum_compute}$ is the time needed to perform the longest current summation and switching action calculations in parallel. From these computational times, the time step is determined by:

$$\Delta t \geq 2MAX(t_{branch}, t_{node}) \quad (5.6)$$

5.3 EVALUATION

In this section, the scalability evaluation of each method implementation is presented. To perform evaluation, a single-bus power system was used as the test case, where the size of the model was increased by cascading converters onto the DC bus incrementally. This model was implemented under each method on the FPGA evaluation board and the estimated resource usage and computational delay reported by Xilinx Vivado for each incrementation.

5.3.1 Setup

As a test case for the scalability evaluation of both LIM and LB-LMC FPGA implementations, the signal bus system model shown in Figure 5.1 was developed under both methods with increasing N number of converters and their corresponding cable segments and loads. For each size of the model, the simulation engine of the model under each simulation method was synthesized and implemented under Xilinx Vivado 2015.4 for Xilinx Virtex-7 485t VC707 evaluation board and the timing and resource usage report generated by said tool was recorded; only the results of the simulation engine and not of any peripheral entities (switch control, analog output) were noted. The size of the model was increased by three converters for every run after the first converter, until the simulation engine of the model could longer fit, either by running out of resources or route paths on the FPGA. The models were synthesized for the fastest clock period (and time step) achievable for a given model size; if a model FPGA implementation could not meet desired

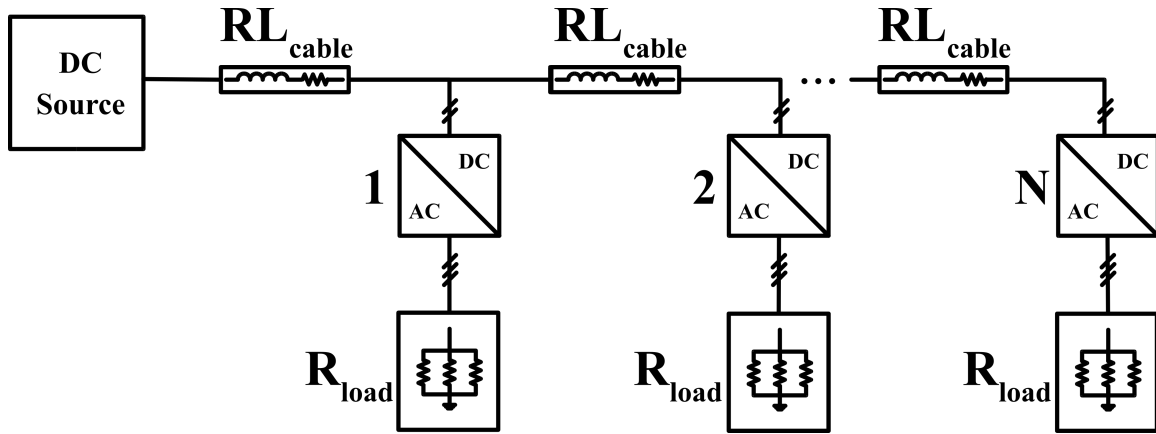


Figure 5.1 Scalability Test Model

timing, the clock period used for the design was increased by 5ns and the design was re-implemented for the new timing. The LB-LMC engine in the test was run in single pass per time step operation and required 72-bit fixed point for precise computation; the LIM engine requires only 64-bit fixed point to achieve similar accuracy as the LB-LMC setup. For N number of converters included in the model under LB-LMC, the number of inductor models for the cable line increased by $2N$ and the number of capacitors for the converter output filtering increased by $3N$. The number of circuit nodes in the model increased by $7N + 2$. Under LIM, both the branch entity and node entity amount increased by $5N$.

5.3.2 LIM Results

The LIM simulation engine scalability results are shown in Figure 5.2 and Table 5.1. The computational delay is the estimated longest time needed by the LIM engine to update one half time step, either the branch half or the node half. As expected, the results show that LIM is very scalable on an FPGA, having linear increase in resources as converters are added to the model, with 140 DSPs and approximately 10000 LUTs needed for every converter and corresponding circuit elements; this usage allowing up to 17 converter models to be instanced on the FPGA.

Table 5.1 LIM Scalability Results

| N | Computational Delay (ns) | Time Step (ns) | LUTs | DSPs |
|----|--------------------------|----------------|--------|------|
| 1 | 18.068 | 40 | 10149 | 140 |
| 4 | 18.281 | 40 | 40478 | 560 |
| 7 | 19.307 | 40 | 70939 | 980 |
| 10 | 19.271 | 40 | 101341 | 1400 |
| 13 | 19.935 | 40 | 131792 | 1820 |
| 16 | 19.963 | 40 | 162634 | 2240 |
| 17 | 19.809 | 40 | 172903 | 2380 |

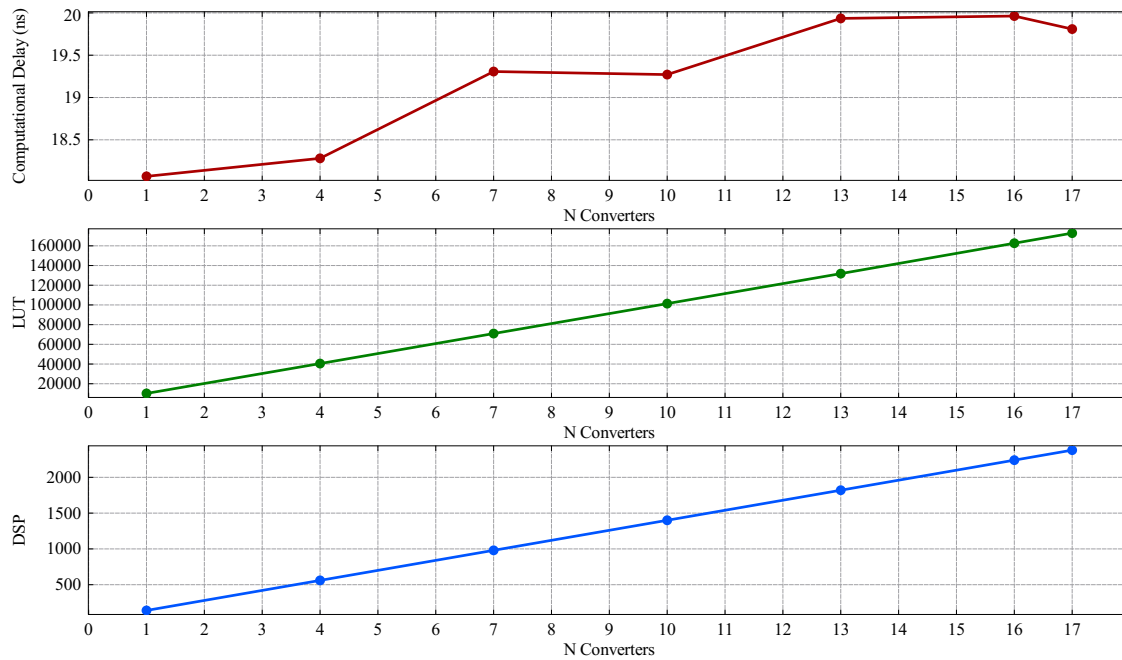


Figure 5.2 Plot of LIM Scalability Results

The computational delay stayed relatively constant for every N of converters included, with delay approximately between 18 and 20 ns, allowing each model size examined to use a 40ns time step. It is suspected that the variation in delay is primarily from routing delays between resources on the FPGA, these delays increasing as resource utilization on the FPGA becomes more congested.

Table 5.2 LB-LMC Scalability Results

| N | Computational Delay (ns) | Time Step (ns) | LUTs | DSPs |
|----|--------------------------|----------------|--------|------|
| 1 | 43.184 | 45 | 8862 | 264 |
| 4 | 44.594 | 45 | 39475 | 963 |
| 7 | 44.503 | 45 | 69347 | 1657 |
| 10 | 45.738 | 45 | 98988 | 2355 |
| 10 | 48.478 | 50 | 105735 | 2354 |

5.3.3 LB-LMC Results

The scalability results for the LB-LMC simulation engine are presented in Figure 5.3 and Table 5.2. As predicted, the resource usage of LB-LMC on FPGA approximately scaled linearly, with LUTs increasing to additional 9925 on average for every new converter added to the model with corresponding elements, and DSPs increasing by 236 on average for every new converter segment cascaded to the model. However, the amount of resources needed for each tested size of the model was higher than that of the LIM engine usage, limiting number of converters to a count of 10. It is expected that the extra resource usage is from needing to use 72-bit fixed point data sizes to keep result accuracy reasonable, which is higher than 64-bit size used by LIM model for similar accuracy. Use of larger word size requires more resources to perform computations. Furthermore, LB-LMC engine uses a system solver that LIM does not have, this solver growing larger as the model size increases and serving as extra overhead to the LB-LMC engine. The computational delay scaled sublinearly as expected like LIM, but minimum time step allowed by the delay was 5ns greater than LIM for same model. Moreover, the computational delay grew at quicker rate than with LIM, causing the model engine to fail desired timing with 10 converters and needing to raise time step to 50ns for this size. At 50ns time step, the model engine needed 48.5ns to reach solutions every time step, higher than 44.5 and 45.7 ns from other runs, though the larger increase is likely from routing delays and effort made by Xilinx Vivado

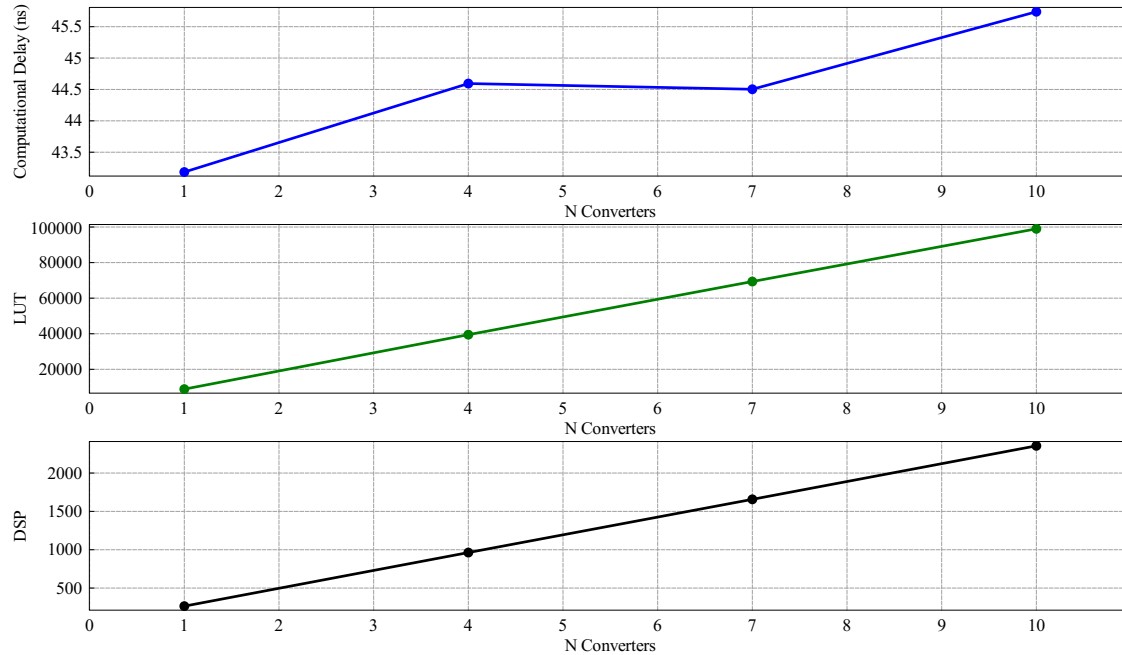


Figure 5.3 Plot of LB-LMC Scalability Results

place-and-route tool to meet given 50ns time step. In any case, the greater increase in computational delay is expected to stem from system equations in the system solver increasing in length as more components and nodes are added to the test model. Though the equations come out to be dataflow computational units where multiplication operations are performed in parallel, the summation of all multiplication results still needs to be accumulated to acquire the final result for a given node voltage. This summation, using dual input addition units for each add, is a sequential process where the result of two additions need to be added together and so forth. As a sequential process, computational delay is expected to increase.

CHAPTER 6

MODELING AND IMPLEMENTATION DISCUSSION

In creating a power system model for FPGA implementation with a given simulation method, it is important to understand the limitations and challenges in getting such models to work in such a setup. Limitations can include, though not limited to, whether a system model can be instanced in a given method, if possible, without significant network transformations and modifications, or whether a model can be executed without becoming numerical instable or inaccurate for given time step or data word size. Other challenges can involve the process of implementing the model on FPGA once said model is created, such as pre-computing system matrices and developing solvers. In this chapter, these limitations and challenges for creating power system models for the FPGA implementations of LB-LMC method and LIM are discussed and compared.

6.1 LB-LMC MODELING ON FPGA

A major limitation of the FPGA implementation of LB-LMC is the system solver. Unlike LIM, LB-LMC requires a system solver that is separate from the circuit component entities that make up a given power system model. This system solver depends on a pre-computed conductance matrix G that describes the conductances of the system network. For every model to be simulated, the conductance matrix, and its inversion G^{-1} , must be computed offline from the LB-LMC simulation engine. As such, if any parameter of the model needs to be altered, say for example the load for a power converter, the matrix must be recomputed every time and

the FPGA implementation needs to be re-synthesized as well; a lengthy process for large system models using existing FPGA synthesis tools. The re-computation and re-synthesis is also required if the time step is changed as the time step is included in calculations of conductances for components with latency, such as capacitors and inductors; this prevents the possibilities of effectively changing the time step of a simulation after a model has been loaded onto a given FPGA.

Beyond the conductance matrix, the system solver also requires modifications or recreation for different or changing system topologies before a model can be synthesized for FPGA execution. As the system topology is altered, the linear equations that model the system will also change, requiring modeling equations in the system solver to be altered. For instance, if new components are added to a model and linked to nodes, the sub-solver of the system solver that accumulates the b vector of the system will need to be modified to take the source contributions from the new components. Furthermore, should non-independent elements be added to a model that instances new nodes in the system network, the size and number of equations as seen in (3.2) will need to be expanded as well.

Despite the issue with the conductance matrix and system solver, LB-LMC is requires little to no modification to a given system model to be implemented in it. Unlike LIM, LB-LMC can support most circuit elements and topologies. This support lies in LB-LMC method's use of linear equations to model and solve system network models, similar to how Resistive Companion (RC) method works which is used in commercial simulation tools such as SPICE. Moreover, due to LB-LMC method's roots from RC method, LB-LMC supports a wide variety of integration methods, implicit/explicit or mixed, to approximate state equations for latency inducing circuit elements to enable desired modeling stability and accuracy for given time step size. These benefits allow LB-LMC to be highly versatile and robust for simulating virtually any power system to be evaluated.

6.2 LIM MODELING ON FPGA

Despite proving to be highly scalable for real-time simulation on FPGA as noted in Chapter 5, LIM does suffer from the issue of requiring rigid topology structure for system models which LB-LMC lacks. In traditional LIM, branches must always be composed of inductor with optional series resistance and voltage source, and nodes must comprise of a capacitor to ground with optional parallel conductance and current source. However, many electrical networks do not fit this structure, such as having capacitors serving as a branch between two nodes. Ideally, most systems can be made to fit LIM structure through network transformations, examples including but not limited to Thevenin and Norton transformations, but some topologies would require overly extensive modifications to be practical. Then, for branches and nodes in a system that contain no latency elements (sources and resistances), latency must be artificially inserted into a model to fit LIM structure, thereby making the model less of an accurate approximation of a given system. For LIM to be more versatile, LIM will need to be expanded with new compatible branch and node entities to enable less rigid topology requirements; such as branch capacitors, node inductors, and non-latency elements.

Along with topology issues, LIM is sensitive to numerical stability for larger time steps or small latencies. Traditional LIM uses an explicit integration to approximate the state equations of the branches and nodes, as seen in (2.7) and (2.9). From this use of explicit integration, should the latency (capacitance or inductance) be significantly smaller than for a given time step, computed solutions for each half time step in LIM can become unstable, causing the model to fail. Though the nanosecond range time steps achievable with LIM on FPGA allow usage of small capacitances and inductances in real-time, instability can arise when attempting to model detailed system models that incorporate all parasitic effects that often are minuscule.

Though LIM is inflexible in system topology and latency inclusion, this method is more robust in FPGA implementation compared to LB-LMC. Not needing a system solver, or related conductance matrix, like LB-LMC, LIM only requires entities for each branch and node for a model to be instanced and then to link them together. Without a large, central element needing to change with the model, component parameters can be more readily altered, including time step. This setup even enables the possibility of changing parameters and time step after a model design has been synthesized and loaded onto a FPGA through replacing the currently used parameter constants with configurable registers or block RAM units on a FPGA. However, should the topology need to change though, the model design will still need to be re-synthesized again.

CHAPTER 7

FUTURE WORK

While the present work on the LB-LMC and LIM implementations on FPGA have brought high-fidelity and scalable tools to simulate power systems, much work can be done to take the implementations further to improve practical usefulness and robustness of said implementations. Currently, the FPGA simulation engines have to be hand-developed for every system model to simulate. For larger models, this development can become tedious and highly error-prone, especially if multiple models have to be instanced. Instead, further work can be done to automatically generate the RTL code for the simulation engines from a given power system model. This work can be done through creating software tools which take the netlist and parameters of a system model and then generate the appropriate code of the simulation engine for the model that can be synthesized for FPGA execution.

Other work that can be performed is expanding development of the multi-pass execution for the LB-LMC simulation engines. In present state, the LB-LMC simulation engine with multi-pass execution gains greatest resource usage reduction when the sub-system solver execution is looped, though usage reduction is not as great as expected. Other attempts of implementing multi-pass execution, including looping the solving of each linear equation in the system solver, have caused resource usage increases beyond using single pass execution. Efforts can be made to reduce resource usage further for multi-pass execution while still maintaining adequate time steps for high frequency switching converter modeling. Moreover, other work can be explored to incorporate pipelined floating-point arithmetic op-

erations into the multi-pass execution to dramatically improve simulation precision and error over using fixed-point arithmetic.

One element that can be improved is the limited versatility of the LIM FPGA implementation. Currently, only inductor branches and capacitor nodes have been implemented as entities in the LIM simulation engine design. While these two entities can model a wide variety of power electronic systems, many other systems cannot be modeled with only these two. For instance, three-phase wye or delta configuration of inductors, commonly seen in power loads, cannot be modeled with the branch entities because the configuration requires inductors to be connected together without nodes entities in-between. Moreover, power converters in full bridge topology that incorporate filter capacitors between switch legs will require a branch capacitor. Other LIM-compatible components, including branch capacitors, node inductors, and transformer elements that are mentioned in [12], can be implemented in the FPGA simulation engine design to enable further amount of power electronic systems to be modeled.

Another thing that can be taken further is optimizing the FPGA simulation engines for reduced resource usage and computational delay. While the scalability of the two methods on FPGA are admirable, the size of the models is still limited by the amount of resources available on FPGAs, keeping potential for extensively sized power system models from existing. Significant reduction of resources, through changing data word size and re-expressing model equations for less operations, can allow larger models to be simulated on FPGA with LB-LMC or LIM. Decrease in computational delay for simulation methods would be also be something to explore in future work to improve scalability of LB-LMC and to reduce time steps below 40ns.

Finally, work can be taken further to enable hardware-in-the-loop (HIL) and power HIL (PHIL) simulation with the simulation engine FPGA implementations

for both methods. The current simulation platform implementation presented in this work could be expanded to allow simulated power electronic systems to interact with physical elements such as closed-loop controller units, AC machines, and more. With the real-time execution of the developed simulation engines and availability of analog IO boards, the potential for HIL simulation for testing with real systems and external closed-loop power system control exists. However, HIL simulation with the engines was not fully explored due to time constraints. This situation can be remedied in future iterations of this work.

CHAPTER 8

CONCLUSION

The demand in scalable, system-level, real-time simulation for power electronic systems has increased in recent years. FPGA implementations of existing latency-based simulation methods, LB-LMC and LIM, were developed, analyzed, and compared to see if they can meet these demands and provide new benefits to high fidelity, real-time simulation. The LB-LMC method was implemented on a Virtex-7 FPGA, with various component entities solving themselves in parallel before having the system solver linearly compute total system solution in single or multiple pass execution per time step. LIM was realized on same FPGA, operating in two-pass, leapfrog execution where all branches update in parallel together during first half time step and then all nodes simultaneously update in second half time step. Switching action of power converters were modeled with altering the voltage and current source terms of the LIM entities during respective half time step update period. After analysis, these two methods implemented on FPGA proved to be highly scalable. The LB-LMC method was able to simulate power systems with up to ten converters, running with time steps between 45 to 50ns. Likewise, LIM implementation was able to simulate systems with up to seventeen converters, running with a time step of 40ns and below for all test cases. Both methods scaled in resource usage linearly for every converter incorporated into the model, though LIM had lesser increase in resources as model size increased when compared to LB-LMC method. Despite the scalability of LIM implementation on FPGA, LIM does suffers from limited versatility of possible system models and numerical in-

stability when latency is too small or time steps are too large for given system dynamics. On the other hand, the LB-LMC method, while suffering from need of a costly system solver that needs to be altered for every system model, is capable of stably modeling a vastly larger variety of power electronic system models with little to no modification to said models due to roots in the widely proven resistive companion method. With the two implementations, new groundwork is made for the progression of system-level, real-time simulation of power electronic systems.

REFERENCES

- [1] L. Bin, X. Wu, H. Figueroa, and A. Monti, "A low-cost real-time hardware-in-the-loop testing approach of power electronics controls," *IEEE Trans. Ind. Electron.*, vol. 54, pp. 919–931, Feb. 2007.
- [2] L. Yunwei, D. Vilathgamuwa, and L. P. Chiang, "Design, analysis, and real-time testing of a controller for multibus microgrid system," *IEEE Trans. Power Electron.*, vol. 19, pp. 1195–1204, May 2005.
- [3] Z. Ivanovic, E. Adžić, M. Vekić, S. Grabić, N. Čelanović, and V. Katić, "Hil evaluation of power flow control strategies for energy storage connected to smart grid under unbalanced conditions," *IEEE Trans. Power Electron.*, vol. 27, pp. 4699–4710, Nov. 2012.
- [4] M. Matar and R. R. Iravani, "FPGA implementation of the power electronic converter model for real-time simulation of electromagnetic transients," *IEEE Trans. Power Del.*, vol. 25, pp. 852–860, Feb. 2010.
- [5] N. R. Tavana and V. Dinavahi, "Real-time nonlinear magnetic equivalent circuit model of induction machine on FPGA for hardware-in-the-loop simulation," *IEEE Trans. Energy Convers.*, vol. 31, pp. 520–530, Feb. 2016.
- [6] J. Liu and V. Dinavahi, "A real-time nonlinear hysteretic power transformer transient model on FPGA," *IEEE Trans. Ind. Electron.*, vol. 61, pp. 1254–1260, Jul. 2014.
- [7] H. Saad, T. Ould-Bachir, J. Mahseredjian, C. Dufour, S. Dennetiere, and S. Nguéfeu, "Real-time simulation of MMCs using CPU and FPGA," *IEEE Trans. Power Electron.*, vol. 30, pp. 259–267, Jan. 2015.
- [8] J. Jin-Hong, K. Jong-Yul, K. Hak-Man, K. Seul-Ki, C. Changhee, K. Jang-Mok, A. Jong-Bo, and N. Keo-Yang, "Development of hardware in-the-loop simulation system for testing operation and control functions of microgrid," *IEEE Trans. Power Electron.*, vol. 25, pp. 2919–2929, Dec. 2010.

- [9] V. Jalili-Marandi, L. Pak, and V. Dinavahi, "Real-time simulation of grid-connected wind farms using physical aggregation," *IEEE Trans. Ind. Electron.*, vol. 57, pp. 3010–3021, Sep. 2010.
- [10] W. Li, G. Joós, and J. Bélanger, "Real-time simulation of a wind turbine generator coupled with a battery supercapacitor energy storage system," *IEEE Trans. Ind. Electron.*, vol. 57, pp. 1137–1145, Apr. 2010.
- [11] A. Benigni and A. Monti, "A parallel approach to real-time simulation of power electronics systems," *IEEE Trans. Power Electron.*, vol. 30, pp. 5192–5206, Sep. 2015.
- [12] J. E. Schutt-Aine, "Latency insertion method (LIM) for the fast transient simulation of large networks," *IEEE Trans. Circuits Syst. I*, vol. 48, pp. 81–89, Jan. 2001.

APPENDIX A

LB-LMC ENGINE HLS C++ CODE

A.1 CAPACITOR ENTITY

```
1 #include "Capacitor.hpp"
2
3 Capacitor::Capacitor(NumType dt, NumType cap)
4 : dt(dt), cap(cap), hoc2(NumType(2.0)*cap/dt)
5 , epos_past(0.0), eneg_past(0.0), delta_v(0.0), delta_v_past(0.0)
6 , current(0.0), current_eq(0.0), current_past(0.0), current_eq_past
  (0.0)
7 {}
8
9 void Capacitor::operator()(NumType epos, NumType eneg, NumType*
  bout)
10 {
11     #pragma HLS inline
12
13     #pragma HLS latency min=0 max=0
14
15     //register past values
16     epos_past = epos;
17     eneg_past = eneg;
18     current_past = current;
19     current_eq_past = current_eq;
20     delta_v_past = delta_v;
21
22     delta_v = AddSubType(epos_past) - AddSubType(eneg_past);
23
24     current = (hoc2)*(delta_v) - (current_eq_past);
25
26     current_eq = (current) + (hoc2)*(delta_v);
27
28     *bout = current_eq;
29 }
```

A.2 INDUCTOR ENTITY

```
1 #include "Inductor.hpp"
2
3 Inductor::Inductor(NumType dt, NumType ind)
4 : dt(dt), ind(ind), hol2(dt/NumType(2.0)/ind)
5 , epos_past(0.0), eneg_past(0.0), delta_v(0.0), delta_v_past(0.0)
6 , current(0.0), current_eq(0.0), current_past(0.0), current_eq_past
  (0.0)
7 {}
8
9 void Inductor::operator()(NumType epos, NumType eneg, NumType*
  bout)
10 {
11     #pragma HLS inline
12
13     #pragma HLS latency min=0 max=0
14
15     //register past values
16     epos_past = epos;
17     eneg_past = eneg;
18     current_past = current;
19     current_eq_past = current_eq;
20     delta_v_past = delta_v;
21
22     delta_v = AddSubType(epos_past) - AddSubType(eneg_past);
23
24     current = hol2*delta_v - current_eq_past;
25
26     current_eq = -current - hol2*delta_v;
27
28     *bout = current_eq;
29 }
```

A.3 THREE PHASE HALF-BRIDGE CONVERTER ENTITY

```
1 #include "ThreePhaseHBConverter.hpp"
2
3 ThreePhaseHBConverter::ThreePhaseHBConverter(NumType dt, NumType
  cap, NumType ind, NumType res)
4 : dt(dt), cap(cap), ind(ind), res(res), hoc(dt/cap), hol(dt/ind),
  cap_conduct(10000.0)
5 , vc1(0.0), vc2(0.0), il1(0.0), il2(0.0), il3(0.0), ipos(0.0), ineg
  (0.0)
6 , epos_past(0.0), eneg_past(0.0), eout1_past(0.0), eout2_past(0.0),
  eout3_past(0.0)
7 , il1_past(0.0), il2_past(0.0), il3_past(0.0), vc1_past(0.0),
  vc2_past(0.0)
```

```

8   ,sw1(false),sw2(false),sw3(false)
9 {}
10
11 void ThreePhaseHBConverter::operator()(NumType epos, NumType eneg
    , NumType eout1, NumType eout2, NumType eout3,
12     NumType* bpos, NumType* bneg, NumType* bout1, NumType* bout2,
    NumType* bout3,
13     bool sw_ctrl1, bool sw_ctrl2, bool sw_ctrl3)
14 {
15     #pragma HLS inline
16
17     #pragma HLS latency min=0 max=0
18
19     epos_past = epos;
20     eneg_past = eneg;
21     eout1_past = eout1;
22     eout2_past = eout2;
23     eout3_past = eout3;
24     il1_past = il1;
25     il2_past = il2;
26     il3_past = il3;
27     vc1_past = vc1;
28     vc2_past = vc2;
29     sw1 = sw_ctrl1;
30     sw2 = sw_ctrl2;
31     sw3 = sw_ctrl3;
32
33     AddSubType a1, a2, a3, b1, b2, b3, a, b, c;
34
35     if(sw1)
36     {
37         a1 = il1_past;
38         b1 = 0.0;
39         a = vc1_past;
40     }
41     else
42     {
43         a1 = 0.0;
44         b1 = il1_past;
45         a = vc2_past;
46     }
47
48     if(sw2)
49     {
50         a2 = il2_past;
51         b2 = 0.0;
52         b = vc1_past;
53     }
54     else
55     {
56         a2 = 0.0;
57         b2 = il2_past;
58         b = vc2_past;
59     }

```

```

60
61  if(sw3)
62  {
63      a3 = il3_past;
64      b3 = 0.0;
65      c = vc1_past;
66  }
67  else
68  {
69      a3 = 0.0;
70      b3 = il3_past;
71      c = vc2_past;
72  }
73
74  ipos = cap_conduct*(AddSubType(epos_past) - AddSubType(vc1_past
    ));
75  ineg = cap_conduct*(AddSubType(eneg_past) - AddSubType(vc2_past
    ));
76
77  il1 = AddSubType(il1_past) + hol*( a - AddSubType(eout1_past) -
    res*(il1_past));
78  il2 = AddSubType(il2_past) + hol*( b - AddSubType(eout2_past) -
    res*(il2_past));
79  il3 = AddSubType(il3_past) + hol*( c - AddSubType(eout3_past) -
    res*(il3_past));
80
81  vc1 = hoc*(AddSubType(ipos) - a1 - a2 - a3) + AddSubType(
    vc1_past);
82  vc2 = hoc*(AddSubType(ineg) - b1 - b2 - b3) + AddSubType(
    vc2_past);
83
84  *bpos = (vc1)*cap_conduct;
85  *bneg = (vc2)*cap_conduct;
86  *bout1 = il1;
87  *bout2 = il2;
88  *bout3 = il3;
89 };

```

A.4 SIMULATION ENGINE FOR MICROGRID (SINGLE BUS SYSTEM)

```

1  #include "MicrogridSimEngine.hpp"
2  #include "../LBMCCComponents.hpp"
3  #include "MicrogridSystemSolver.hpp"
4
5  void MicrogridSimEngine(bool inv_swctrl_a, bool inv_swctrl_b,
    bool inv_swctrl_c, NumType bout[23], NumType vout[23])
6  {
7      const static NumType dt      = 60.0e-9; // time step length (s)
8      const static NumType vg      = 1000.0 ; // input generator/
    source voltage

```

```

9   const static NumType rg      = 0.001 ;    // input generator/
    source series resistance
10  const static NumType line_l  = 0.0001 ;  // line/bus
    inductance per segment
11  const static NumType line_r  = 0.1 ;     // line/bus series
    resistance per segment
12  const static NumType inv_cin  = 0.001 ;  // input bus
    capacitance of 3p inverters
13  const static NumType inv_cfilt = 1.0e-6 ; // output
    capacitance of 3p inverters
14  const static NumType inv_lfilt = 0.0001 ; // output
    inductance of 3p inverters
15  const static NumType inv_rfilt = 0.0 ;   // output series
    resistance of 3p inverters
16  const static NumType load_r   = 10.0 ;   // load resistance of
    the inverters
17
18  ////////////////////////////////////////////////////
19  // signals
20
21  NumType inv_b[15];
22  NumType cap_b[9];
23  NumType ind_b[6];
24  NumType srcv_b[2];
25
26  static NumType v[23]; //zero indexed, so v[0] = v1
27
28  ////////////////////////////////////////////////////
29  //components
30
31  srcv_b[0] = vg/rg;
32  srcv_b[1] = vg/rg;
33
34  static Inductor l01(dt, line_l);
35  static Inductor l02(dt, line_l);
36  static Inductor l03(dt, line_l);
37  static Inductor l04(dt, line_l);
38  static Inductor l05(dt, line_l);
39  static Inductor l06(dt, line_l);
40
41  static ThreePhaseHBCConverter inv1(dt, inv_cin, inv_lfilt,
    inv_rfilt);
42  static ThreePhaseHBCConverter inv2(dt, inv_cin, inv_lfilt,
    inv_rfilt);
43  static ThreePhaseHBCConverter inv3(dt, inv_cin, inv_lfilt,
    inv_rfilt);
44
45  static Capacitor c01(dt, inv_cfilt);
46  static Capacitor c02(dt, inv_cfilt);
47  static Capacitor c03(dt, inv_cfilt);
48  static Capacitor c04(dt, inv_cfilt);
49  static Capacitor c05(dt, inv_cfilt);
50  static Capacitor c06(dt, inv_cfilt);
51  static Capacitor c07(dt, inv_cfilt);

```

```

52  static Capacitor c08(dt, inv_cfilt);
53  static Capacitor c09(dt, inv_cfilt);
54
55  ///////////////////////////////////////////////////////////////////
56  //simulation loop
57
58  l01(v[ 0],v[ 1], ind_b+ 0);
59  l02(v[ 2],v[ 3], ind_b+ 1);
60  l03(v[ 4],v[ 5], ind_b+ 2);
61  l04(v[ 7],v[ 8], ind_b+ 3);
62  l05(v[ 9],v[10], ind_b+ 4);
63  l06(v[11],v[12], ind_b+ 5);
64
65  inv1(v[ 2],v[ 9],v[14],v[15],v[16],inv_b+ 0,inv_b+ 1,inv_b+ 2,
        inv_b+ 3,inv_b+ 4,inv_swctrl_a,inv_swctrl_b,inv_swctrl_c);
66  inv2(v[ 4],v[11],v[17],v[18],v[19],inv_b+ 5,inv_b+ 6,inv_b+ 7,
        inv_b+ 8,inv_b+ 9,inv_swctrl_a,inv_swctrl_b,inv_swctrl_c);
67  inv3(v[ 6],v[13],v[20],v[21],v[22],inv_b+10,inv_b+11,inv_b+12,
        inv_b+13,inv_b+14,inv_swctrl_a,inv_swctrl_b,inv_swctrl_c);
68
69  c01(v[14], 0.0, cap_b+0);
70  c02(v[15], 0.0, cap_b+1);
71  c03(v[16], 0.0, cap_b+2);
72  c04(v[17], 0.0, cap_b+3);
73  c05(v[18], 0.0, cap_b+4);
74  c06(v[19], 0.0, cap_b+5);
75  c07(v[20], 0.0, cap_b+6);
76  c08(v[21], 0.0, cap_b+7);
77  c09(v[22], 0.0, cap_b+8);
78
79  MicrogridSystemSolver(inv_b, cap_b, ind_b, srcv_b, bout, v);
80
81  //output solution vector
82  for(int i = 0; i<23;i++)
83  {
84      #pragma HLS UNROLL
85
86      vout[i] = v[i];
87  }
88 }

```

A.5 SYSTEM SOLVER FOR MICROGRID (SINGLE BUS SYSTEM)

```

1  #include "MicrogridSystemSolver.hpp"
2
3  void MicrogridSystemSolver(NumType inv_b[15], NumType cap_b[9],
        NumType ind_b[6], NumType srcv_b[2], NumType bout[23],
        NumType v[23])
4  {
5      #pragma HLS INTERFACE ap_none port=inv_b

```

```

6  #pragma HLS ARRAY_PARTITION variable=inv_b dim=1
7  #pragma HLS INTERFACE ap_none port=cap_b
8  #pragma HLS ARRAY_PARTITION variable=cap_b dim=1
9  #pragma HLS INTERFACE ap_none port=ind_b
10 #pragma HLS ARRAY_PARTITION variable=ind_b dim=1
11 #pragma HLS INTERFACE ap_none port=srcv_b
12 #pragma HLS ARRAY_PARTITION variable=srcv_b dim=1
13
14 #pragma HLS ARRAY_PARTITION variable=bout dim=1
15 #pragma HLS ARRAY_PARTITION variable=v dim=1
16
17 NumType v_block1[7];
18 NumType v_block2[7];
19 NumType v_independ[9];
20
21 NumType b[23];
22 NumType b_block1[7];
23 NumType b_block2[7];
24 NumType b_independ[9];
25
26 //solve for source vector b from component b contributions
27 bVectorSolverMicrogrid(inv_b, cap_b, ind_b, srcv_b, b);
28
29 //break out b vector elements for solvers
30 for(int i = 0; i < 7; i++)
31 {
32     #pragma HLS UNROLL
33
34     b_block1[i] = b[i];
35     b_block2[i] = b[i+7];
36 }
37
38 b_independ[0] = b[14];
39 b_independ[1] = b[15];
40 b_independ[2] = b[16];
41 b_independ[3] = b[17];
42 b_independ[4] = b[18];
43 b_independ[5] = b[19];
44 b_independ[6] = b[20];
45 b_independ[7] = b[21];
46 b_independ[8] = b[22];
47
48 //solve the voltage solutions
49 vBlockSolverMicrogrid(b_block1, v_block1);
50 vBlockSolverMicrogrid(b_block2, v_block2);
51 vIndependentSolverMicrogrid(b_independ, v_independ);
52
53 //feed out the outputs
54 v[ 0] = v_block1[0];
55 v[ 1] = v_block1[1];
56 v[ 2] = v_block1[2];
57 v[ 3] = v_block1[3];
58 v[ 4] = v_block1[4];
59 v[ 5] = v_block1[5];

```



```

60 v[ 6] = v_block1[6];
61
62 v[ 7] = v_block2[0];
63 v[ 8] = v_block2[1];
64 v[ 9] = v_block2[2];
65 v[10] = v_block2[3];
66 v[11] = v_block2[4];
67 v[12] = v_block2[5];
68 v[13] = v_block2[6];
69
70 v[14] = v_independ[0];
71 v[15] = v_independ[1];
72 v[16] = v_independ[2];
73 v[17] = v_independ[3];
74 v[18] = v_independ[4];
75 v[19] = v_independ[5];
76 v[20] = v_independ[6];
77 v[21] = v_independ[7];
78 v[22] = v_independ[8];
79
80 //feed out b vector for external logging
81 for(int i=0; i<23;i++)
82 {
83     #pragma HLS UNROLL
84
85     bout[i] = b[i];
86 }
87 }
88
89 void bVectorSolverMicrogrid(NumType inv_b[15], NumType cap_b[9],
    NumType ind_b[6], NumType srcv_b[2], NumType b[23])
90 {
91     #pragma HLS ARRAY_PARTITION variable=inv_b dim=1
92     #pragma HLS ARRAY_PARTITION variable=cap_b dim=1
93     #pragma HLS ARRAY_PARTITION variable=ind_b dim=1
94     #pragma HLS ARRAY_PARTITION variable=srcv_b dim=1
95     #pragma HLS ARRAY_PARTITION variable=b dim=1
96
97     b[ 0] = srcv_b[0] + ind_b[0];
98     b[ 1] = -ind_b[0];
99     b[ 2] = inv_b[0*5 + 0] + ind_b[1];
100    b[ 3] = -ind_b[1];
101    b[ 4] = inv_b[1*5 + 0] + ind_b[2];
102    b[ 5] = -ind_b[2];
103    b[ 6] = inv_b[2*5 + 0];
104
105    b[ 7] = ind_b[3] - srcv_b[1];
106    b[ 8] = -ind_b[3];
107    b[ 9] = inv_b[0*5 + 1] + ind_b[4];
108    b[10] = -ind_b[4];
109    b[11] = inv_b[1*5 + 1] + ind_b[5];
110    b[12] = -ind_b[5];
111    b[13] = inv_b[2*5 + 1];
112

```

```

113 b[14] = inv_b[0*5+2] + cap_b[0];
114 b[15] = inv_b[0*5+3] + cap_b[1];
115 b[16] = inv_b[0*5+4] + cap_b[2];
116
117 b[17] = inv_b[1*5+2] + cap_b[3];
118 b[18] = inv_b[1*5+3] + cap_b[4];
119 b[19] = inv_b[1*5+4] + cap_b[5];
120
121 b[20] = inv_b[2*5+2] + cap_b[6];
122 b[21] = inv_b[2*5+3] + cap_b[7];
123 b[22] = inv_b[2*5+4] + cap_b[8];
124
125 }
126
127 void vIndependentSolverMicrogrid(NumType b_independ[9], NumType
    v_independ[9])
128 {
129 #pragma HLS ARRAY_PARTITION variable=b_independ dim=1
130 #pragma HLS ARRAY_PARTITION variable=v_independ dim=1
131
132 for(int i = 0; i<9; i++)
133 {
134 #pragma HLS UNROLL
135 v_independ[i] = b_independ[i]*Microgrid_A_independent;
136 }
137 }
138
139 void vBlockSolverMicrogrid0Loop(NumType b_block[7], NumType
    v_block[7])
140 {
141 #pragma HLS ARRAY_PARTITION variable=b_block dim=1
142 #pragma HLS ARRAY_PARTITION variable=v_block dim=1
143
144 for(int i=0;i<7;i++)
145 {
146 #pragma HLS UNROLL
147
148 v_block[i] = b_block[0]*Microgrid_A_block[i][0] + b_block
149 [1]*Microgrid_A_block[i][1] + b_block[2]*Microgrid_A_block[i]
    [2] + b_block[3]*Microgrid_A_block[i][3] +
    b_block[4]*Microgrid_A_block[i][4] + b_block
150 [5]*Microgrid_A_block[i][5] + b_block[6]*Microgrid_A_block[i]
    [6];
151 }
152
153 void vBlockSolverMicrogrid7Loop(NumType b_block[7], NumType
    v_block[7])
154 {
155 #pragma HLS ARRAY_PARTITION variable=b_block dim=1
156 #pragma HLS ARRAY_PARTITION variable=v_block dim=1
157
158 NumType t[7] = { 0,0,0,0,0,0,0 };
159

```

```
160 for(int i = 0; i<7; i++)
161 {
162     #pragma HLS PIPELINE II=1
163
164     for(int j = 0; j<7; j++)
165     {
166         #pragma HLS UNROLL
167         t[j] = b_block[i]*Microgrid_A_block[j][i] + t[j];
168     }
169 }
170
171 for(int i = 0; i < 7; i++)
172 {
173     #pragma HLS UNROLL
174     v_block[i] = t[i];
175 }
176 }
```

APPENDIX B

LIM ENGINE HLS C++ CODE

B.1 BRANCH ENTITY

```
1 #include "LIMBranch.hpp"
2
3 LIMBranch::LIMBranch(NumType l, NumType r, NumType dt) :
4   l(l), r(r), dt(dt), hol(dt/l), k(NumType(1.0) - hol*r), i_past
5   (0.0)
6 {}
7 void LIMBranch::update(NumType vi, NumType vj, NumType e, NumType
8   * i)
9 {
10  #pragma HLS latency min=0 max=0
11  #pragma HLS inline off
12
13  i_past = i_past*k + hol*(vi - vj + e);
14  *i = i_past;
15 }
```

B.2 NODE ENTITY

```
1 #include "LIMNode.hpp"
2
3 LIMNode::LIMNode(NumType g, NumType c, NumType dt) :
4   g(g), c(c), dt(dt), divc(NumType(1.0)/(c/dt + g)), coh(c/dt),
5   v_past(0.0)
6 {}
7 void LIMNode::update(NumType i_sum, NumType h, NumType* v)
8 {
9  #pragma HLS latency min=0 max=0
10  #pragma HLS inline off
11
12  v_past = divc*( (coh*v_past) + (h - i_sum) );
13  *v = v_past;
14 }
```

B.3 SIMULATION ENGINE FOR MICROGRID (SINGLE BUS SYSTEM)

```
1 #include "MicrogridModel.hpp"
2 #include "../LIMParams.hpp"
3 #include <ap_utils.h>
4
5 void MicrogridModel(bool swa, bool swb, bool swc, NumType vout
6 [17], NumType iout[15])
7 {
8     #pragma HLS ARRAY_PARTITION variable=vout dim=1
9     #pragma HLS ARRAY_PARTITION variable=iout dim=1
10
11     #pragma HLS latency min=1 max=1
12
13     //parameters //////////////////////////////////////
14     const static NumType dt = LIM_Timestep;
15
16     const static NumType vg = 6000.0;
17
18     const static NumType inv_lfilt = 0.0001;
19     const static NumType inv_cfilt = 1.0e-6;
20     const static NumType inv_rfilt = 0.0;
21     const static NumType inv_cin = 0.001;
22     const static NumType load_g = 1.0/7.0; // 1.0/load_r
23
24     const static NumType line_l = 1.0e-5;
25     const static NumType line_r = 0.01;
26
27     //////////////////////////////////////
28
29     //input voltage sources //////////////////////////////////////
30     const static NumType vgp = vg;
31     const static NumType vgn = -vg;
32
33     //bus branches //////////////////////////////////////
34
35     static LIMBranch bus_b1(line_l, line_r, dt);
36     static LIMBranch bus_b2(line_l, line_r, dt);
37     static LIMBranch bus_b3(line_l, line_r, dt);
38     static LIMBranch bus_b4(line_l, line_r, dt);
39     static LIMBranch bus_b5(line_l, line_r, dt);
40     static LIMBranch bus_b6(line_l, line_r, dt);
41
42     //converter elements //////////////////////////////////////
43
44     static LIMBranch inv1_ba(inv_lfilt, inv_rfilt, dt);
45     static LIMBranch inv1_bb(inv_lfilt, inv_rfilt, dt);
46     static LIMBranch inv1_bc(inv_lfilt, inv_rfilt, dt);
47     static LIMNode inv1_cinp(0.0, inv_cin, dt);
48     static LIMNode inv1_cinn(0.0, inv_cin, dt);
49     static LIMNode inv1_loada(load_g, inv_cfilt, dt);
```

```

50 static LIMNode   inv1_loadb(load_g, inv_cfilt, dt);
51 static LIMNode   inv1_loadc(load_g, inv_cfilt, dt);
52
53 static LIMBranch inv2_ba(inv_lfilt, inv_rfilt, dt);
54 static LIMBranch inv2_bb(inv_lfilt, inv_rfilt, dt);
55 static LIMBranch inv2_bc(inv_lfilt, inv_rfilt, dt);
56 static LIMNode   inv2_cinp(0.0, inv_cin, dt);
57 static LIMNode   inv2_cinn(0.0, inv_cin, dt);
58 static LIMNode   inv2_loada(load_g, inv_cfilt, dt);
59 static LIMNode   inv2_loadb(load_g, inv_cfilt, dt);
60 static LIMNode   inv2_loadc(load_g, inv_cfilt, dt);
61
62 static LIMBranch inv3_ba(inv_lfilt, inv_rfilt, dt);
63 static LIMBranch inv3_bb(inv_lfilt, inv_rfilt, dt);
64 static LIMBranch inv3_bc(inv_lfilt, inv_rfilt, dt);
65 static LIMNode   inv3_cinp(0.0, inv_cin, dt);
66 static LIMNode   inv3_cinn(0.0, inv_cin, dt);
67 static LIMNode   inv3_loada(load_g, inv_cfilt, dt);
68 static LIMNode   inv3_loadb(load_g, inv_cfilt, dt);
69 static LIMNode   inv3_loadc(load_g, inv_cfilt, dt);
70
71 //currents and voltages //////////////////////////////////
72 static NumType voltages[17];
73 static NumType currents[15];
74
75 //internal voltages and currents //////////
76 static NumType inv1_isums[5];
77 static NumType inv1_e[3];
78 static NumType inv1_h[2];
79 static NumType inv2_isums[5];
80 static NumType inv2_e[3];
81 static NumType inv2_h[2];
82 static NumType inv3_isums[5];
83 static NumType inv3_e[3];
84 static NumType inv3_h[2];
85
86 NumType
87 inv1_a1, inv1_a2, inv1_a3, inv1_b1, inv1_b2, inv1_b3, inv1_x1,
   inv1_x2, inv1_y1, inv1_y2, inv1_z1, inv1_z2,
88 inv2_a1, inv2_a2, inv2_a3, inv2_b1, inv2_b2, inv2_b3, inv2_x1,
   inv2_x2, inv2_y1, inv2_y2, inv2_z1, inv2_z2,
89 inv3_a1, inv3_a2, inv3_a3, inv3_b1, inv3_b2, inv3_b3, inv3_x1,
   inv3_x2, inv3_y1, inv3_y2, inv3_z1, inv3_z2;
90
91 //////////////////////////////////////////
92 //////////////////////////////////////////
93
94 //update   //////////////////////////////////
95
96 { //stage 1
97     #pragma HLS protocol floating
98     #pragma HLS latency min=0 max=0
99     //switching action
100

```

```

101         //branches
102     bus_b1.update(voltages[0],voltages[1], 0.0,currents + 0);
103     bus_b2.update(voltages[1],voltages[2], 0.0,currents + 1);
104     bus_b3.update(voltages[2],voltages[3], 0.0,currents + 2);
105     bus_b4.update(voltages[4],voltages[5], 0.0,currents + 3);
106     bus_b5.update(voltages[5],voltages[6], 0.0,currents + 4);
107     bus_b6.update(voltages[6],voltages[7], 0.0,currents + 5);
108
109     if(swa)
110     {
111         inv1_x1 = voltages[1];
112         inv2_x1 = voltages[2];
113         inv3_x1 = voltages[3];
114     }
115     else
116     {
117         inv1_x1 = voltages[5];
118         inv2_x1 = voltages[6];
119         inv3_x1 = voltages[7];
120     }
121     //-----
122     if(swb)
123     {
124         inv1_y1 = voltages[1];
125         inv2_y1 = voltages[2];
126         inv3_y1 = voltages[3];
127     }
128     else
129     {
130         inv1_y1 = voltages[5];
131         inv2_y1 = voltages[6];
132         inv3_y1 = voltages[7];
133     }
134     //-----
135     if(swc)
136     {
137         inv1_z1 = voltages[1];
138         inv2_z1 = voltages[2];
139         inv3_z1 = voltages[3];
140     }
141     else
142     {
143         inv1_z1 = voltages[5];
144         inv2_z1 = voltages[6];
145         inv3_z1 = voltages[7];
146     }
147
148     inv1_e[0] = inv1_x1 ;
149     inv1_e[1] = inv1_y1 ;
150     inv1_e[2] = inv1_z1 ;
151     inv2_e[0] = inv2_x1 ;
152     inv2_e[1] = inv2_y1 ;
153     inv2_e[2] = inv2_z1 ;
154     inv3_e[0] = inv3_x1 ;

```

```

155     inv3_e[1] = inv3_y1 ;
156     inv3_e[2] = inv3_z1 ;
157
158     inv1_ba.update(0.0,voltages[ 8],inv1_e[0],currents + 6);
159     inv1_bb.update(0.0,voltages[ 9],inv1_e[1],currents + 7);
160     inv1_bc.update(0.0,voltages[10],inv1_e[2],currents + 8);
161     inv2_ba.update(0.0,voltages[11],inv2_e[0],currents + 9);
162     inv2_bb.update(0.0,voltages[12],inv2_e[1],currents + 10);
163     inv2_bc.update(0.0,voltages[13],inv2_e[2],currents + 11);
164     inv3_ba.update(0.0,voltages[14],inv3_e[0],currents + 12);
165     inv3_bb.update(0.0,voltages[15],inv3_e[1],currents + 13);
166     inv3_bc.update(0.0,voltages[16],inv3_e[2],currents + 14);
167
168 } //end stage 1
169
170 { //stage 2
171     #pragma HLS protocol floating
172     //currents entering/exiting nodes
173     inv1_isums[0] = -currents[0] + currents[1];
174     inv1_isums[1] = -currents[3] + currents[4];
175     inv1_isums[2] = -currents[6];
176     inv1_isums[3] = -currents[7];
177     inv1_isums[4] = -currents[8];
178
179     inv2_isums[0] = -currents[1] + currents[2];
180     inv2_isums[1] = -currents[4] + currents[5];
181     inv2_isums[2] = -currents[9];
182     inv2_isums[3] = -currents[10];
183     inv2_isums[4] = -currents[11];
184
185     inv3_isums[0] = -currents[2];
186     inv3_isums[1] = -currents[5];
187     inv3_isums[2] = -currents[12];
188     inv3_isums[3] = -currents[13];
189     inv3_isums[4] = -currents[14];
190
191     if(swa)
192     {
193         inv1_a1 = currents[6];
194         inv1_b1 = 0.0;
195
196         inv2_a1 = currents[9];
197         inv2_b1 = 0.0;
198
199         inv3_a1 = currents[12];
200         inv3_b1 = 0.0;
201     }
202     else
203     {
204         inv1_a1 = 0.0;
205         inv1_b1 = currents[6];
206
207         inv2_a1 = 0.0;
208         inv2_b1 = currents[9];

```



```

209
210     inv3_a1 = 0.0;
211     inv3_b1 = currents [12];
212 }
213 // -----
214 if (swb)
215 {
216     inv1_a2 = currents [7];
217     inv1_b2 = 0.0;
218
219     inv2_a2 = currents [10];
220     inv2_b2 = 0.0;
221
222     inv3_a2 = currents [13];
223     inv3_b2 = 0.0;
224 }
225 else
226 {
227     inv1_a2 = 0.0;
228     inv1_b2 = currents [7];
229
230     inv2_a2 = 0.0;
231     inv2_b2 = currents [10];
232
233     inv3_a2 = 0.0;
234     inv3_b2 = currents [13];
235 }
236 // -----
237 if (swc)
238 {
239     inv1_a3 = currents [8];
240     inv1_b3 = 0.0;
241
242     inv2_a3 = currents [11];
243     inv2_b3 = 0.0;
244
245     inv3_a3 = currents [14];
246     inv3_b3 = 0.0;
247 }
248 else
249 {
250     inv1_a3 = 0.0;
251     inv1_b3 = currents [8];
252
253     inv2_a3 = 0.0;
254     inv2_b3 = currents [11];
255
256     inv3_a3 = 0.0;
257     inv3_b3 = currents [14];
258 }
259
260     inv1_h [0] = -inv1_a1 - inv1_a2 - inv1_a3;
261     inv1_h [1] = -inv1_b1 - inv1_b2 - inv1_b3;
262     inv2_h [0] = -inv2_a1 - inv2_a2 - inv2_a3;

```

```

263     inv2_h[1] = -inv2_b1 - inv2_b2 - inv2_b3;
264     inv3_h[0] = -inv3_a1 - inv3_a2 - inv3_a3;
265     inv3_h[1] = -inv3_b1 - inv3_b2 - inv3_b3;
266
267     //nodes
268     voltages[0] = vgp;
269     voltages[4] = vgn;
270
271     inv1_cinp.update( inv1_isums[0],inv1_h[0],voltages + 1);
272     inv1_cinn.update( inv1_isums[1],inv1_h[1],voltages + 5);
273     inv1_loada.update(inv1_isums[2],0.0,voltages + 8);
274     inv1_loadb.update(inv1_isums[3],0.0,voltages + 9);
275     inv1_loadc.update(inv1_isums[4],0.0,voltages + 10);
276
277     inv2_cinp.update( inv2_isums[0],inv2_h[0],voltages + 2);
278     inv2_cinn.update( inv2_isums[1],inv2_h[1],voltages + 6);
279     inv2_loada.update(inv2_isums[2],0.0,voltages + 11);
280     inv2_loadb.update(inv2_isums[3],0.0,voltages + 12);
281     inv2_loadc.update(inv2_isums[4],0.0,voltages + 13);
282
283     inv3_cinp.update( inv3_isums[0],inv3_h[0],voltages + 3);
284     inv3_cinn.update( inv3_isums[1],inv3_h[1],voltages + 7);
285     inv3_loada.update(inv3_isums[2],0.0,voltages + 14);
286     inv3_loadb.update(inv3_isums[3],0.0,voltages + 15);
287     inv3_loadc.update(inv3_isums[4],0.0,voltages + 16);
288
289     //feed out the outputs //////////////////////////////////
290
291     for(int i = 0; i < 17; i++)
292     {
293         #pragma HLS unroll
294
295         vout[i] = voltages[i];
296     }
297
298     for(int i = 0; i < 15; i++)
299     {
300         #pragma HLS unroll
301
302         iout[i] = currents[i];
303     }
304 } //end stage 2
305 }

```